POLITECNICO DI TORINO

Department of Control and Computer Engineering

Master of Science degree in

Mechatronic Engineering

Study and design of a bioinspired actuation system for a soft robotic total artificial heart

Supervisors

Marcello Chiaberge

Matteo Cianchetti

Cecilia Laschi

Candidate

Debora Zrinscak

September, 2018

If you are thinking of an idea that
you can solve in your lifetime,
you are thinking too small.

Abstract

With an average of 75 beats per minute, 4,500 beats an hour, 108,000 per day, 39,400,000 in a year, and more than 3 billion beats per lifetime: the heart is undoubtedly one of the most fascinating organs in our bodies. Thanks to its tireless and powerful pumping functionality, indeed, it is responsible of blood oxygenation and circulation throughout our whole life.

Pathologic conditions related to the cardiovascular system present, for this reason, a particularly high index of mortality. In fact, despite all the technological advances, every year 26 million people die because of heart failures, leaving, thus, the disease at the first place as single source of death worldwide.

The main reason behind such a frightening scenario is the fact that the only solution to the problem is a heart transplant: the donors shortage and the unavailability of an artificial device, able to permanently substitute its natural functionality, then, increase incredibly the number of patients dying during the await.

To date, depending on the severity of the pathologic condition, a ventricular assist device or a total artificial heart can be implanted. These devices can be both pulsatile or continuous-flow, electrically, magnetically, fluidically driven. The only FDA-certified total artificial heart device commercially available is the Syncardia TAH, a pneumatic pump, supplied by percutaneous drivelines. Although it reportedly brought to a high number of successful heart transplants, its use is limited to bridge-to-transplant applications, since the longest survival registered as destination therapy is around, but less than, four years.

In the last years, however, due to the interest arising out of a growing research in the soft robotics field, completely different solutions have been engineered. By exploiting the use of soft materials, reconfigurable and scalable smart actuation technologies, and bioinspired motions, this new research area seems to be promising in the artificial organs field. Although farsighted, the so far presented devices are still far from being implantable: they opened, however, a completely new and incredibly stimulating range of thinkable solutions.

This work, thus, aims to design a bioinspired actuation system for a novel typology of soft total artificial heart. In this framework, the studies of the Spanish scientist Francisco Torrent-Guasp represent the solid basis for its development. Indeed, by demonstrating that

the myocardium is a unique muscular band, sequentially activating and folded in double helix, Torrent-Guasp unrevealed also the incredible embodied intelligence of this organ. Taking inspiration from this discovery, in this thesis, a simplified geometrical model of the left ventricular chamber and its surrounding muscular arrangement will be presented and discussed, enabling, then, a thoughtful actuating technology choice. The artificial muscular fibre, indeed, will need to have muscle-like contraction characteristics, miniaturization possibilities, sequential activation abilities and present low risks for health in case of future implantability.

Along with the considerations about the future models for the control of the muscular sequential activation, the possibly employable soft sensor solutions will be exposed.

Thanks to its innovative nature, this work lays the foundations for of a novel, bioinspired and fully soft total artificial heart, thus bringing new hopes to the endless research of the heart failures ultimate therapy.

Table of contents

Table of Figures

List of Tables

1 Introduction

A powerful asymmetric pump, a self-activating muscle: our heart, because of its important function, yet its complex working mechanisms, is probably one of the most fascinating organs in our bodies.

Since antiquity, indeed, it has been thoroughly studied: already in the 4th century, philosophers as Aristoteles believed it to be the centre of motion, intelligence and sensation of every living being.

With the Renaissance, anatomy was then rediscovered thanks to the revival of the ancient writings, and thus further investigations and observations clarified the working principles and basic structures of the organs. This allowed to build a wide and accurate knowledge about the heart, already in the 17th century.

To better understand the motivations behind this work, and the underlying working principles, an introduction to the anatomy, the possible diseases and solutions is fundamental.

1.1 Anatomy

1.1.1 Basic notions

The human heart is a cone-shaped muscle, of a dimension of a fist, and an average weight of 250-350 grams in adults. It is located just behind and slightly left the breastbone. It is composed by four chambers: two smaller ones, called atria, positioned on top of two larger ones called ventricles.

The longitudinal axis divides the muscle into right and left heart. The right heart (RH) is responsible of receiving blood from the systemic circulation through the right atrium

(RA), and of its subsequent oxygenation, thanks to the pumping action of the right ventricle (RV), pushing it into the lungs.

The left heart (LH), instead, receives the oxygenated blood from the pulmonary circulation, through the left atrium (LA), and it pumps it to all the organs and tissues of the body thanks to the powerful action of the left ventricle (LV).

The activation of the two atria is simultaneous and alternated to the contraction of the two ventricles: this creates a rhythmic alternation of contraction phases, called systoles, and relaxation ones, called diastoles. A complete cycle is thus known as cardiac cycle, and it will be analysed thoroughly later on.

The main function of the two atria is to collect the blood from the other organs of the body: the RA receives it thanks to the inferior and superior venae cavae, while the LA through the pulmonary vein. Because of this, their walls present less myocardial tissue than the ventricular ones, resulting in reduced wall thickness. The atrial systolic phase, being less powerful, thus, just helps the blood to flow into the ventricular cavity.

This passage is regulated by the presence of two important valves: the tricuspid valve, connecting the two chambers of the RH, and the mitral or bicuspid connecting LA and LV.

As shown in Fig.1, there are also two other valves, called, because of their particular shape, semilunar valves. They regulate the periodic ejection of the blood from the two ventricles towards the lungs, for what concerns the RV, and towards the systemic circulation for the LV.

1.1.2 The myocardium

In the human body, the heart is the organ responsible of the blood oxygenation and circulation. Its important pumping task is made possible thanks to the particular kind of muscular fibres that compose the cardiac muscle. Known as myofibrils, indeed, they are the fundamental actuation element of the third typology of muscular fibres along with the skeletal and smooth ones: the myocardium. This typology is characterized by an involuntary activation, similar to the smooth ones, but a striated appearance and power, as in the skeletal ones.

The myocardium composes the thick mid-layer between the external heart wall, called epicardium, and the internal one, called endocardium. It is supplied by the coronary vessels surrounding the muscle.

The basic element of this kind of muscle are the cardiac cells, called cardiomyocytes, joined together thanks to intercalated discs, encased by collagen fibres. There are two types of cardiac cells: one represents the basic contractile element, while the other, constituting just 1% of the overall amount, is responsible of the rhythmical electrical activation, also known as pace-maker cells.

Typically, healthy cardiomyocytes are generally cylindrical, 100µm long, 10-25µm wide in diameter, and their main feature is linked to the ability of spontaneous depolarization, causing a longer refractory period between subsequent activations. This particular behaviour prevents from the hyperstimulation of the cardiac muscle.
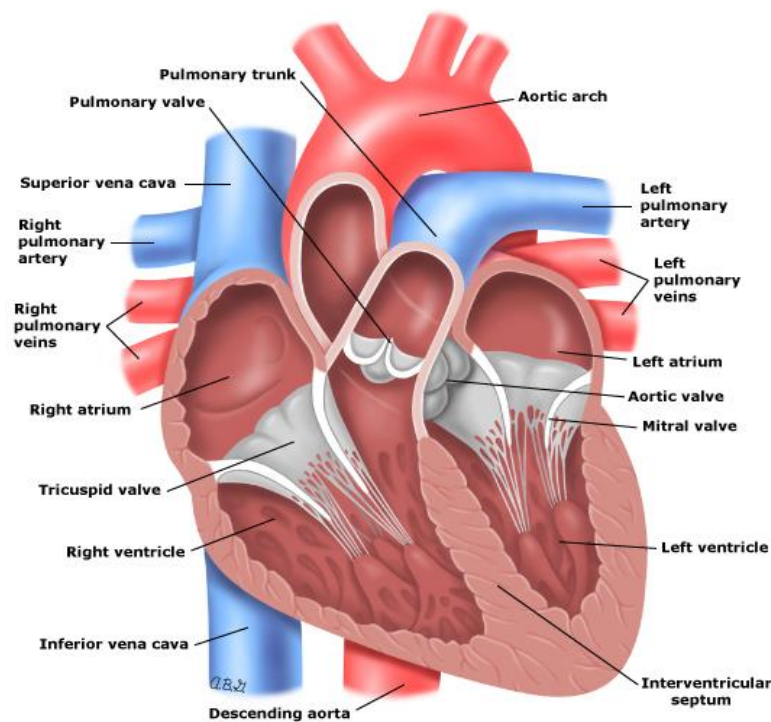
Fig. 1 Basic cardiac anatomy

Even if the cardiac pacemaker cells represent a small minority, the presence of intercalated disks, and thus connective tissue, assures the congruent contraction of every cardiomyocyte. The alternative contraction and relaxation of myofibrils, bundles of cardiac cells, generates the typical cardiac cycle with subsequent systolic and diastolic phases. [1]

1.1.3 Cardiac Cycle
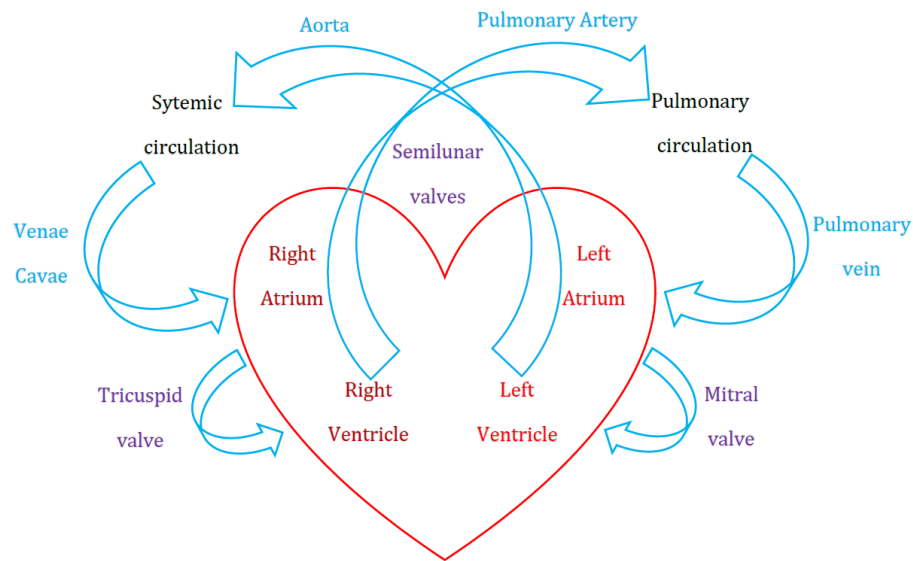
Fig. 2 Main stages of the cardiac cycle

For clarity, Fig.2 illustrates the main stages of a cardiac cycle.

In Fig.3, the time-pressure and time-volume diagrams of an average LH cardiac cycle are shown, along with the most important physiological values.

The main points depicted in the first diagram are listed and explained hereafter:

①. Beginning of atrial contraction: pressure rises.

②. Blood ejection from the atria towards the ventricle, through the tricuspid valve: pressure decreases.

③. End of atrial systole: atrioventricular (AV) valve closes [C] thanks to a slight depressurization of the chamber. Start of the ventricular rapid filling.

④. End of ventricular filling and beginning of the ventricular isovolumetric contraction: pressure increase causing the opening of the aortic valve [A].

⑤. Ventricular ejection occurs when the pressure inside the LV overcomes the systemic one generally around 120 mmHg.

⑥. Semilunar valve closes [B], causing a secondary upstroke in the aortic pressure wave called Dicrotic notch.

⑦. Decrease of pressure in the ventricular cavity due to the isovolumetric relaxation phase.

⑧. The left atrioventricular valve opens [D]: passive atrial filling occurs.
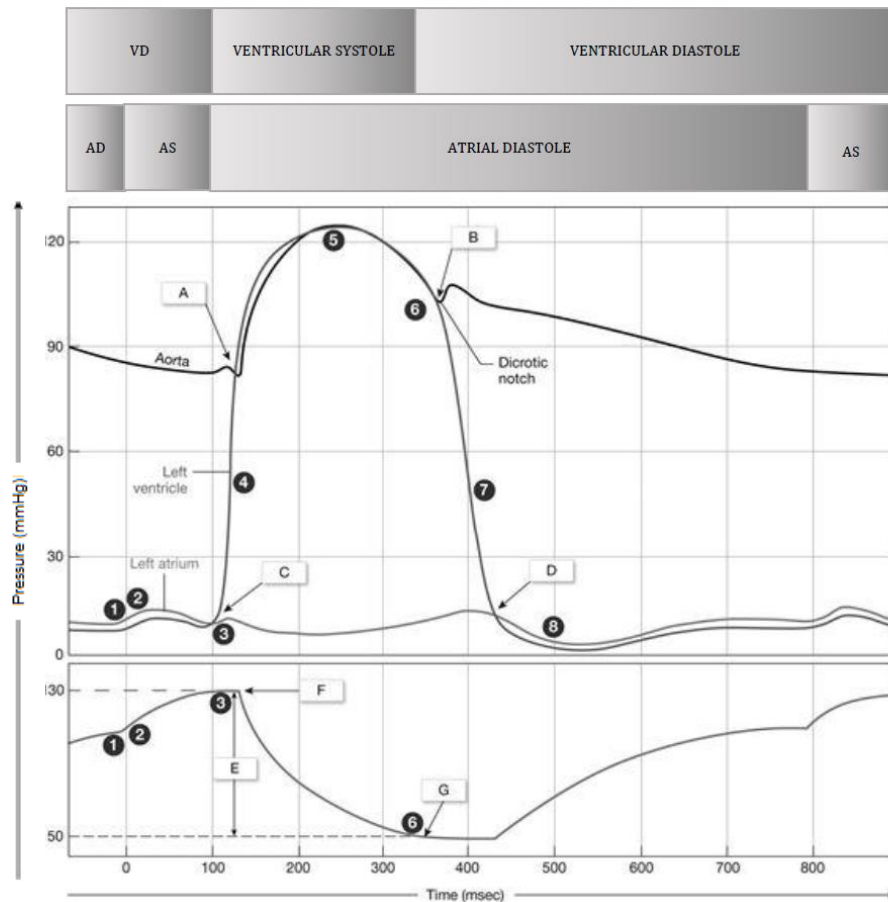
Fig. 3 Pressure and volume evolution during the cardiac cycle

A similar diagram can be drawn for the right heart as well: in this case, however, the minimum pressure in diastole is around 10 mmHg, instead of 15 mmHg, and the maximum pressure value reached after the isovolumic contraction of the ventricle, known as afterload, is defined by the pulmonary artery, and it is around 25 mmHg. This significant difference between the two ventricular systolic pressures determines also a different wall composition. In order to be able to generate higher internal forces, the left ventricle is also generally characterized by a thicker layer of myocardial tissue.

As evident from the above explanation, the cardiac can be generally subdivided into two phases: systole and diastole. Its beginning is set, by convention, at the end of the diastole. Systole is defined as from the mitral valve closure to the aortic valve closure, while the rest is usually called diastole. By observing the myocardial physiology, however, the definition of diastole includes portions of cycle that could be considered systole. Hence, the systole can be subdivided into two phases: (1) isovolumetric contraction and

(2) ejection, while the diastole into four: (1) isovolumetric relaxation, (2) early diastolic filling, (3) diastasis and (4) atrial filling [2].

For what concerns time intervals, it is possible to notice that a normal cardiac cycle lasts around 800 ms. However, the duration of systolic and diastolic period, in both atria and ventricles, is significantly different: systole lasts around 300 ms in ventricles and around 100 ms in atria, while the diastole takes around 500 ms in ventricles and 700 ms in atria.

The second diagram in Fig, 4, shows, instead, the corresponding relation between the left ventricular internal volume and cardiac cycle timing. [E] represents the stroke volume (SV), defined as difference between end-diastolic volume (EDV) and the end-systolic (ESV) one.

$$SV = EDV - EDS$$

Note that, the EDV is defined as the volume of blood present inside the ventricle, corresponding to the AV valve closure: it is also known as preload volume, since it stretches the ventricle to its maximum dimensions under variable physiologic conditions. It is important to observe that this value depends also on the venous return value (VR). The VR is defined as the amount of blood flowing back into the ventricles. The EDS, instead, is the volume left after the semilunar valve closure. In average, the EDV is computed to be around 130 ml, EDS around 50 ml, and thus the SV around 80 ml. It is trivial to say that these values can vary, depending on the age, sex and health of the single individual, taken into consideration.

From the definition of SV, it is possible to define another important value: the cardiac ejection fraction (EF).

$$EF\% = \frac{SV}{EDV} * 100$$

This value, usually lays around 70% in a healthy heart, and it is significant when analysing the consequences generated by diseases affecting the cardiac tissue, thus causing, a loss in efficiency of the cardiac pumping functionality.

Considering then that in a healthy individual the heart beats at a rate (HR) of 60-100 bpm, the produced cardiac output (CO) is in average of 5 L/min.

$$CO = SV * HR$$

It is easy to notice that the cardiac output can be incremented both by increasing the stroke volume or the heart rate.

1.1.4 Preload and the Frank-Starling relation

When considering the cardiac hemodynamic working principles, one of the most important relations is the Frank-Starling mechanism, that puts into relation the values of cardiac output and the end diastolic volume, through the length and tension of the myocardium.

The law states that the stroke volume of the heart increases in response to an increase in the volume of blood in the ventricles, before contraction (EDV), when all the other factors remain constant. As a larger volume of blood flows into the ventricle, the blood stretches the cardiac muscle fibres, leading to an increase in the force of contraction. This mechanism allows the CO to be synchronized with the venous return, arterial blood supply and humoral length, without depending upon external regulation to make alterations. In physiology, this results in a maintained balance between right and left ventricular output equality; if it would not exist blood would accumulate into the pulmonary or systemic circulation.

This mechanism is a useful tool to describe the pathologic conditions altering the normal cardiac function, since in health, the heart operates within a range of preload conditions that acutely affect performances. This results in a curve shifted upward and leftward.

In disease conditions, instead, this relationship is depressed downward and rightward so that despite fluid retention and increased preload the subsequent contraction is less vigorous.

Fig. 4 illustrates the above exposed conditions, through a representation of a Frank-Starling curves family.

1.1.5 Afterload and Laplace law

As already stated, the afterload can be defined as the "load" that the heart must eject blood against, and it is closely related to the aortic pressure and the muscular fibres conditions. For this reason, it is usually expressed as wall stress σ

$$\sigma \propto \frac{P * r}{h}$$

where P is the ventricular pressure, r the ventricular radius and h the wall thickness. An increase of afterload results into a depressed Frank-Starling curve, that corresponds to a decreased stroke volume and a simultaneous increase of the left ventricular end-diastolic pressure.

The physical reason of this phenomenon is found in the force-velocity relationship of the myocytes: an increase of afterload, causes a decrease in velocity in fibres shortening. Since the shortening time, and thus ejection, is limited, a decrease in fibre shortening velocity results in a limited ejection fraction and a consequent increase of EDV, that adds up to the values of VR. Inevitably, this condition leads to a
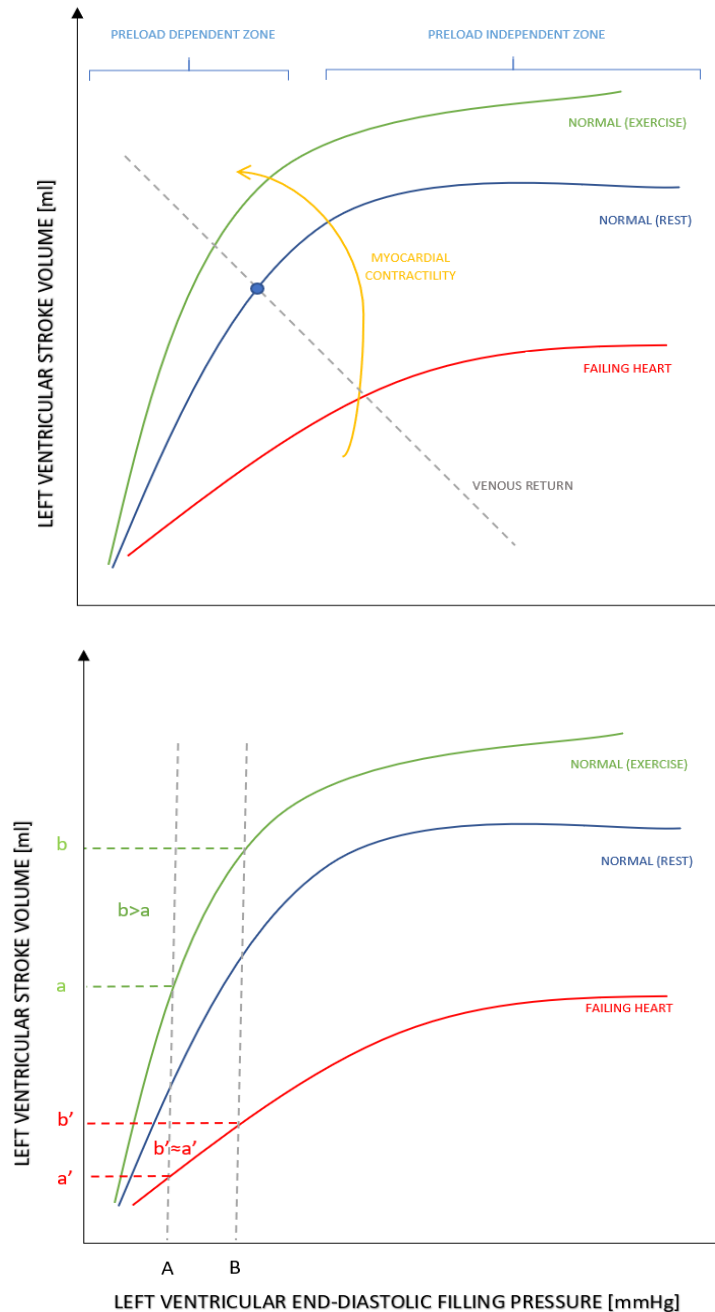
Fig. 4 Family of Frank-Starling curves showing the alterations in the relation between the left ventricular end-diastolic filling pressure and the stroke volume

congestive heart failure.

In contrast, a decrease in afterload shifts the Frank-Starling curve upwards and leftwards, increasing the SV and reducing at the same time the left ventricular end-diastolic pressure.

In Fig. 5 the above explained conditions are illustrated with a pressure-volume diagram, and its modifications.
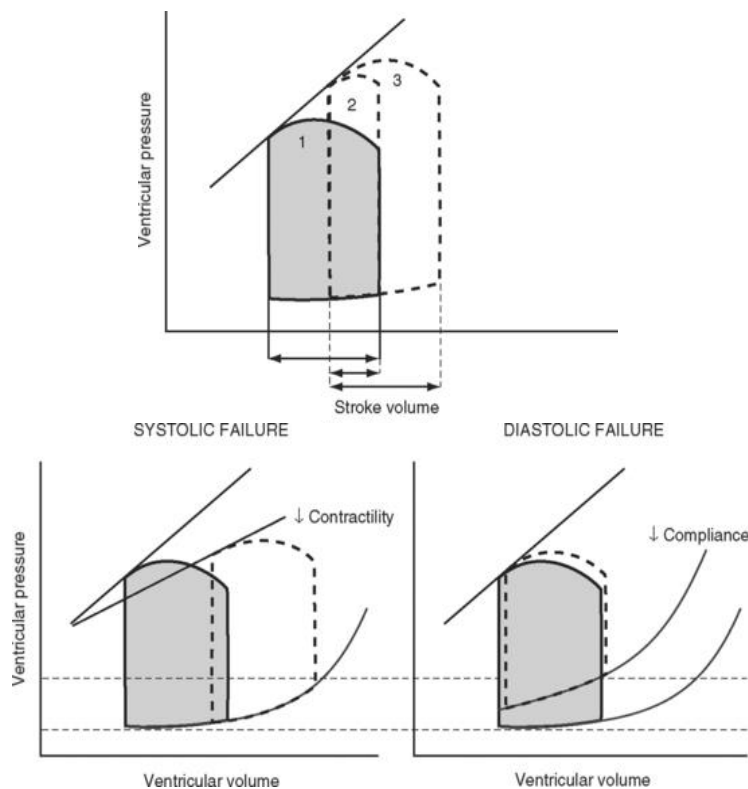
Fig. 5 Modifications of the cardiac cycle curve, due to pathologic conditions

1.2 Cardiovascular Diseases

Cardiovascular diseases (CVDs), are the number one cause of death in the world. Indeed, they usually lead to high morbidity conditions as stroke or heart failure (HF). For the sake of this work, aiming to study a new bioinspired soft robotic total artificial heart, only the diseases causing heart failures will be analysed.

Heart failure, indeed, is the particular condition in which the cardiac muscle is unable to pump efficiently blood in order to maintain the physiological body's requirements: this can be due to either its impossibility to contract, i.e. ventricular systolic dysfunction, HF with reduced ejection fraction (HFrEF), or relax properly, i.e. diastolic dysfunction, HF with preserved ejection fraction disease (HFpEF). The P-V diagram of such conditions can be observed in Fig. 5.

It is important to notice that, so far, in the most critical cases the only available definitive solution to the problem is a heart transplant.

The most common cause of heart failure is the ischaemic heart disease (IHD), also known as myocardial infarction or heart attack. It causes the myocardial tissue death. IHD can be caused by other CVDs as the coronary artery disease, where the congestion of the vessels supplying the heart causes an abnormal blood flow to the tissues. Other causes can be high blood pressure, cardiac arrhythmias, as atrial fibrillation, valvular heart disease, infections, and other unknown cardiomyopathies. All these CVDs can be either caused by congenital conditions, genetic predispositions, or related to some unhealthy lifestyle habits as poor nutrition as obesity, high blood cholesterol, diabetes, tobacco and/or alcohol abuse, and lack of exercise.

HF is also known as "congestive heart failure", since the inability to pump inefficiently blood results is fluid retention in tissues, veins, or other parts of the body, causing oedema, both peripheral and pulmonary.

For these reasons, the main symptoms correlated to this disease are usually excessive tiredness, breath shortness and leg swelling; while, usually, chest pain, including angina, usually does not occur.

The failure can be left-sided, right-sided or biventricular. The left heart is responsible, as already explained, to pump blood into the body after receiving it from the pulmonary circulation. A backward failure of this side would back up the blood into the lungs, causing the typical breath shortness, a forward failure, instead, could cause dizziness and confusion.

The right side, instead, is responsible of the blood oxygenation, thus a backward failure could cause a systemic capillary congestion and consequent swelling.

Although, it can be one-sided, it is more frequent that a biventricular failure occurs. This is also due to the fact that a one sided-failure will necessarily tend to increase stress on the other side.

1.3 Heart Failure Statistics

Being able to understand in deep the functionalities of the heart has always been one of the most inspiring and stimulating challenges of all times. Historically, indeed, the ancient societies, as Egyptians, Greeks and Romans, were already attributing to this organ a central role in our lives: sometimes relating it with both emotions and intelligence.

In the following centuries, then, thanks to the technological advances, scientist had been able to study it more closely, understand its functionalities, but also, lately, observe its complex motion in a living body. All this information, then, confirmed the importance of its role and rose the awareness around the urgent need of an artificial device able to replicate its functionalities.

Cardiovascular diseases (CVDs) and, in particular, congestive heart failures (HF), indeed, are still the principal cause of mortality worldwide: causing about 26 million deaths every year [3]. The American Heart Society and the European Heart Network estimated respectively that annually in the US 5.7 million people develop a HF [4], and 3.9 million people, 45% of the overall amount, die in the EU because of a CVDs [5]. Alarming data that involve both men and women, and that seem to get worse every year [6][7].

The reason behind this dramatic situation is that the only effective solution to this pathologic condition is a heart transplant. However, due to the shortage of donors, just 5000 operations are performed annually, about 2000 of which are done in the US [8].

Moreover, before transplantation, many are the aspects that need to be considered, e.g. the dimensions, the blood type, medical conditions: checks that might cause the impossibility to implant the donor's heart, even if present. Luckily, 73% of the recipients live for 5 years, and 21% up to 20 years after transplantation [9].

It is clear that the situation could be incredibly improved if there was a device, employable as end therapy, able to completely substitute the ventricular pumping

functionality, consequently lowering the number of people still waiting for a donor. In fact, 45% of these patients die while waiting for a donor [10].

Although, many were the efforts made in this direction in the past decades, this possibility, unfortunately, is still far from becoming applicable: no total artificial heart (TAH) has been deemed sufficiently reliable yet. For this reason, most of the commercially available devices are certified by the Food and Drug Association (FDA) as bridge-to-transplantation (BTT) solutions: they mainly aim to sustain or substitute the weakened pumping functionality of the failing heart while waiting for a donor.

Depending on the severity of the patient's conditions, ventricular assist devices (VADs) or total artificial hearts (TAHs) can be employed. VADs are usually implanted when just one of the ventricles, usually the left (LVAD), is damaged and unable to contract properly. The survival rates at one year, linked to the last generation ones, are of an encouraging 86% [11], leaving open, however, the possibility of developing a right heart failure, due to the difficult coordination between the two pumping chambers.

For end-stage patients or those who developed a right heart failure, if all the requirements are met, biventricular assist devices or total artificial hearts are implanted. Survival rates at one year are slightly lower, 80%, however, if one thinks that they were first claimed as destination therapy devices, and the longest given support was of 1374 days, i.e. less than 4 years [12], it is clear that BTT is still the only application possible.

2 State of the art

2.1 Hard Robotic Devices

In order to sustain patients awaiting heart transplantation, to facilitate recovery in patients suffering from reversible cardiac dysfunction, and to provide permanent circulatory support in patients with end-stage heart-failure (HF) who are not candidates for transplantation, so far different devices were engineered.

Depending on the level of diseased myocardial tissue, indeed, the heart pumping functionality can be just partly externally assisted, e.g. by using ventricular assist devices (VADs), or, in the worst cases, completely substituted, with the employment of total artificial hearts (TAHs).

For a sake of completeness both cases will be treated, with a major focus on the second case.

2.1.1 Ventricular Assist Devices (VADs)

Ventricular assist devices (VAD) are systems able to sustain and prolong life in HF patients by assisting the ventricular pumping functionality. Because of the importance of the left ventricular action, and the higher working pressures, the most used VADs are left ventricular assist devices (LVADs).

Since the early 1960s they kept being sought and implanted, and after showing a 1-year doubled survival rate (51% from 25%) in end-stage HF patients, they were FDA approved in the mid-1990s. With further technological advances, by 2011, 85% of patients survived the first year with VAD as BTT. [10]

In general, to date, three are the generations of developed devices. The first one is characterized by positive volume displacement pumps: the blood output is ejected periodically by generating a pulse, thus the name "pulsatile pumps". The most important devices are HeartMate I® (Thoratec Corp., Pleasanton, CA), Thoratec PVAD™ (Thoratec Corp., Pleasanton,CA) and Novacor N100 (World Heart Inc., Oakland, CA). Even though the survival rates were promising, most of the reported complications were related either

to malfunctions of the device, e.g. tear and wear of the moving parts, or to a low biocompatibility, e.g. consequent cloth formations, thrombogenicity. Thus, to decrease the number of moving parts and all the associated problems, the afterwards generation became mostly composed by continuous flow pumps. To mention some: HeartMate II® (Thoratec Corp., Pleasanton, CA), Jarvik 2000 (Jarvik Heart, Inc., New York, NY) and Micromed DeBakey® (MicroMed Cardiovascular, Inc., Houston, TX).

The main discussion that arose around these VADs was about the possible complications of a non-pulsatile system in case of long-term utilization: since no relevant data underlined the connection between continuous flow pumps outputs and prolonged implantations, the necessity of a physiologically-like pulsatile system remains unclear.
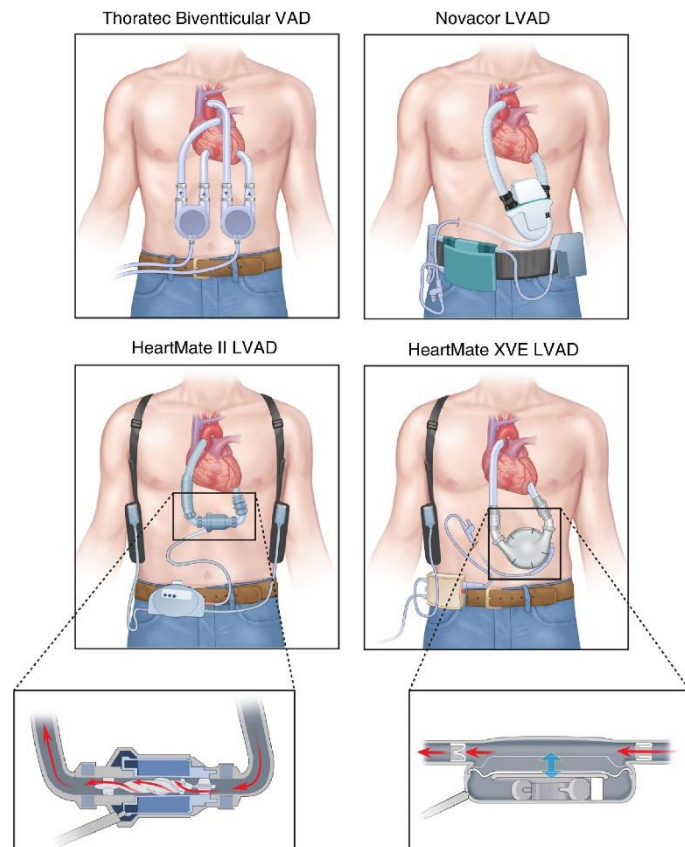
Fig. 6 Representation of the most used Ventricular Assist Devices.

Nevertheless, these VADs became very popular and generally preferred to the previous solutions, more than 90% in 2016 [8], maybe also thanks to some statistic studies involving HeartMate II® that reported very high survival rates [13].

The last generation devices are still generally belonging to the continuous flow pumps group, even if, apart from one exception, the preferred actuation mechanism is a radial or centrifugal flow pump, sometimes also introducing magnetic levitation (MAGLEV) bearings, to further reduce possible frictions and malfunctions. DuraHeart™ (Terumo Heart, Inc., Ann Arbor, MI) [14], HeartWare HVAD® (HeartWare International, Inc., Framingham MA) [15], Incor®, the only axial flow pump (Berlin Heart, Inc., Berlin, Germany) [16], Levacor® (World Heart Inc., Salt Lake City, UT) [17], and HeartMate III (Thoratec Corp., Pleasanton, CA) are just some examples [18].

2.1.2 Total Artificial Hearts (TAHs)

So far, the scientific research focused on the development of a devices able to replicate the basic functionalities of the cardiac muscle. Frequently, for this reason, the results are bulky pumps, made of hard materials, made biocompatible by the employment of treated membranes covering the parts contacting with blood and other organs.

Focusing more in detail on the already available solutions, some of the most promising devices can be listed.

2.1.2.1   SYNCARDIA SYSTEMS INC, Jarvik 7, CardioWest, Syncardia

The first one, shown in Fig.7, is the only so far commercially available: SynCardia™ (SynCardia Systems, Inc., Tucson, AZ, USA). Initially named Jarvick 7, was one of the first devices successfully implanted, after the initial trial with the Dacron TAH in 1969 [19]. To date, the device has been successfully implanted in more than 1300 patients, and in 2014 it also received the FDA approval to start clinical trials as DT device in the US [20].

Fig. 7 Syncardia, the only FDA-approved commercially availabe total artificial heart

SynCardia is a pneumatically driven system and consists of three component elements: (1) the ventricles—independent right and left spherical blood pumping chambers implanted intra-thoracically, (2) drivelines— to connect the TAH ventricles to an external pneumatic driver system and (3) the driver— a pneumatic pumping system allowing coordinated but independent and pulsatile pumping of the ventricles. The external control system dimensions were decreased in the past years, to guarantee a better portability and, thus, patients' life quality. The pulsatile output flow can reach also more than 9L/min.

The ventricles composing the implantable unit, contacting with blood, are separated from the pneumatically-actuated chamber by means of a multi-layered membrane, that prevents the contact between air and blood in case of tear. The dome-like structure is fabricated from segmented polyurethane solution (SPUS) overlaying a Dacron™ Mesh.

The SPUS diaphragms, obtained by sequential pouring over a mould, are lubricated by microparticulate graphite.

By pressurizing the actuation chamber, the membrane moves upwards, pushing the blood towards the outflow valve, emptying the ventricular cavity. Once the systolic phase is over, the ventricles are filled thanks to the membrane backward movement, starting the diastolic phase. The resulting flow is, thus, pulsatile.

For what concerns the driver units, different were the so far developed: ranging from the hospital to the portable ones. The hospital-based console is a large driver unit composed by air tanks, two pneumatic drivers, batteries, alarm system and a computer monitoring the parameters of both ventricles. The % systole, the beat rate and control pressure are manually controlled. These parameters are usually set once during the early post-implant period, and hardly changed later. The cardiac output, based on the artificial chamber airflow, is continuously displayed as the driving pressure.

In operation the primary driver is set to fully eject blood at each beat: for the right ventricle this is achieved by setting the ejection pressure 30 mmHg higher than the pulmonary artery one, while for the left ventricle this results in a 60 mmHg higher pressure with respect to the systemic one. However, the ventricles are not fully filled, a10-20 ml volume is left in order to prevent pulmonary oedema in case of venous return, for example when the patient exercises. Indeed, in this condition, an augmented cardiac output is required in order to supply a higher physiological demand. As previously anticipated, outputs greater than 9 L/min can be easily achieved.

2.1.2.2   CARMAT, C-TAH

The CARMAT (CARMAT SA, Vélizy-Villacoublay, France) researchers, instead, focused more on the biocompatibility of the employed materials, to lower the risks of thrombogenicity and improve the hemocompatibility of the device. Shown in Fig.8, C-TAH was the result of these studies: an electrically powered, but hydraulically actuated pump [21].

Each of the two ventricles consist of two chambers separated by a hybrid membrane. On one side of the membrane, silicone oil activates a rotary pump, displacing back and forth the membrane itself, on the other side, there is the pumping chamber filled with blood. This side of the membrane is made of chemically treated bovine pericardial tissue.

Electronics and microprocessors that drive the device are incorporated into the C-TAH. Sensors in the ventricles allow instantaneous monitoring of pressure: the position of the membrane is detected in situ by ultrasound transducers. Energy is provided by lithium ion batteries carried in a wearable bag or belt connected to the C-TAH by a single transcutaneous highly flexible driveline. The output pulsatile blood flow ranges from 2 L/min to 9 L/min with automated adjustment to balance the ejection between right and left chamber, housing 65 ml of blood each. The maximum volume of actuating fluid is of 750 ml at maximum.

The device presents some important advantages with respect to the commonly used SynCardia, as, in particular, a upgraded biocompatibility of the internal membranes and employed valves, reducing significantly the risk of thrombogenicity and bleeding. However, the bulkiness of the device, make it suitable only for 85% of men and 14% of women, and the need of a percutaneous powering driveline maintains all the problems related to infections. Moreover, the fact that all the microelectronics and moving parts are embedded inside the device, even if on one side improve the ease of implant, on the other make impossible its maintenance without complete explant in case of membrane tear, mechanical parts wear or electronics malfunction.

After being successfully implanted in four patients, and a short period of suspended studies, its development was resumed in 2017 [22].

Fig. 8 The CARMAT C-TAH.

2.1.2.3   ABIOMED, ABIOCOR

Important efforts were made in relation also with the complete implantability of the TAH. Indeed, both the above-mentioned devices are characterized by transcutaneous drivelines, that dramatically increase the probability of infections in case of long term implantations. The first device that needs to be mentioned is the AbioCor® (AbioMed Inc.,

Danvers, MA, USA), an electrohydraulic pump, claimed as "the first self-contained internal TAH", Fig.9 [23]. Indeed, a transcutaneous energy transfer system, allows to power the device without skin perforation. The system is composed by implantable elements, shown in Fig.10, as: (1) a thoracic unit, (2) an internal controller, (3) an internal coil (TET system), and (4) batteries, but also by external elements as 5) a console, 6) a communication box, and a 7) external TET coil.

Fig. 9 The ABIOMED, AbioCor

The thoracic unit is a titanium-made case, with two blood-pumping compartments, harbouring a flexible poly-urethane sac with trileaflet inflow and outflow valves. The flow is alternative and generated by a centrifugal pump agitating a low-viscosity fluid stored between the two sacks. The direction of the fluid is controlled by a rotary valve, depending on the set heart rate. Because of a 55 ml stroke volume, the device beats at 110-140 beats/min.

The controller unit monitors the parameters, including the hydraulic chamber pressure, speed and beating rate, in order to maintain the balance between the two atrial pressures.

The internal batteries can provide power supply up to 45 minutes if completely charged. Otherwise the system is powered through a TET system partly internally implanted, positioned in the sub-pectoral region, and coupled with the external circuit converting electrical power into magnetic.

The console displays the performance parameters allowing manual adjustment, thanks to a radiofrequency communication box, transmitting and receiving information to and from the thoracic unit.

The main advantages of the system are the absence of trans-corporeal drivelines, and an overall reduced

Fig. 10 The overall Abiocor implantable system

operational noise. However, there are some drawbacks, as the bulkiness of the device that limits implantability, questionable biocompatibility, because of high thrombosis risks, 1-2 years maintenance-free life, and non-decouplable and dependant ventricular pumping.

AbioCor received the FDA approval as Humanitarian Device Exception (HDE) in 2006 [24], but the company abandoned further developments the following year because of thromboembolic complications and atrial suck-down events [13].

2.1.2.4   AACHEN UNIVERSITY, REINHEART

Another device, employing the TET circuit is ReinHeart® (Aachen University, Germany), an electromechanical pump [25]. Indeed, the main design requirements were the complete implantability and high durability of the drive and control system. This lead to the development of an electrically powered low-wear linear drive, with a 5-year maintenance-free life, and a less than 20 W required transcutaneously transmitted power.

The system, shown in Fig. 12, is composed by (1) a pump unit, Fig.11, (2) an internal and external controller, (3) an internal and external coil (TET system), (4) a compliance chamber, and (5) batteries. The pump unit is the central element of the system, since it substitutes both anatomically and functionally the native ventricles. Indeed, it is composed by two artificial ventricles, separated from the drive unit by a polyurethane membrane. The pulsatile flow is generated by a magnetic system able to move alternatively, and thus displacing the membrane, that pushes the blood from the two inlet

cuffs, one per chamber, to the two outlet ones. Unidirectional blood flow is helped by the presence of four heart valves.

Focusing on the drive unit, the linear drive is composed by four coils mounted on a bobbin, and magnets. The bobbin is them pulled into or pushed out of the magnetic field by a variation of coil current. Unlike it happens in the natural heart, the overall movement is guided by one

Fig. 11 The ReinHeart pump unit

central axle ejecting alternatively from left and right ventricle.

The actuator is provided by a position-sensing system and a temperature sensor. As seems evident, the only moving parts, subject to wear, are thus the connection springs and the bobbin, feature that ensures durability. Moreover, to prevent from suction effects, and be preload sensitive, the pusher plates are not fixed onto the membranes.

The implantable controller, instead, has three main purposes: 1) power and control the pump unit and the compliance chamber, allowing a controlled filling, but also 2) to provide status information, and, finally 3) provide backup battery power in case of failure. The system is generally supplied by the TET system coil; however, it can support the device for about 45 min at full capacity.

The dimensions of the TET coil are 70 mm for what concerns the outer diameter of the implantable unit, while the external annular one, has the same inner one, but a 100 mm outer one. At optimal coupling, power losses are low and local heating is minimized: the maximal misalignment supported is of 30 mm.

Moreover, externally, the system is also provided with a user interface, and other battery packs. The system, indeed, can be powered either through a power cord for stationary use or through a two battery packs, each weighing less than 1 kg, for a total support up to 12 h, 18 h if a third pack is added. At the present development state, the

overall dimensions are: a diameter of 87 mm, a height of 90 mm, a volume of 550 ml, and a weight 940 g. The maximum stroke volume is set at 60ml

The development and testing are still ongoing. So far, fluid structure interaction simulations, durability, mock circulation loops and animal trials are being performed. In a bovine model, the TAH effectively replaced the heart's function for up to 2 days: flow and pressures were normal, however long-term hemocompatibility is yet to be validated.

The self-contained structure, a bigger volume, along with the complete implantability of the system, and high durability could bring big advantages with respect to the SynCardia device. However, the 90-days animal trial still has to be completed and there are some possibly occurring complications related to the misalignment of the TET powering systems.
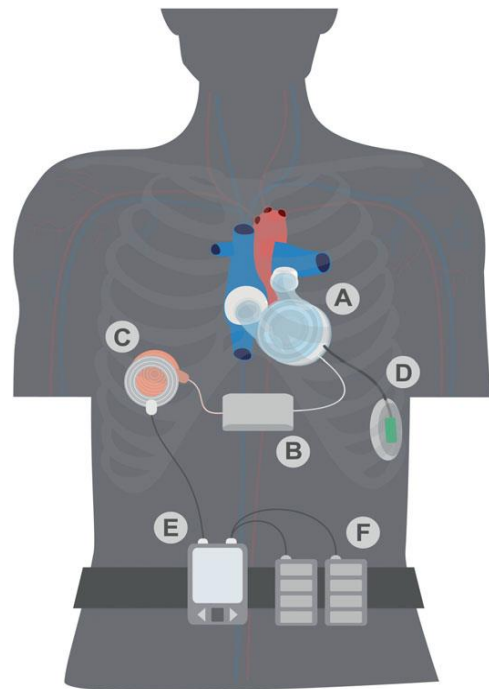
Fig. 12 The overall ReinHeart system. A) pump unit, B) internal controller, C) TET internal and external coils D) compliance chamber E) user interface F)external

2.2 Soft Robotic Devices

Apart from the already mentioned devices, thanks to the increasing curiosity and research around the emerging soft robotics field, alternative devices were presented in the last years. Even if far from being implanted, they introduced the possibility of a different kind of solution, shedding new hopes for the future of TAHs and end-stage HF patients.

When talking about high power density soft pumps, Schumacher et al. [26], presented a heart-inspired one actuated thanks to gas combustion, shown in Fig.13. Although, it was not claimed as possible future TAH, it seems important to mention such a device. Indeed, this pump was able to run >10 000 actuation cycles, displacing a volume of water against a back-pressure of 0.1 bar (75 mmHg).

This heart inspired pump was obtained through a 3D printing lost-wax process: vulcanizing silicone elastomer mixture (PDMS) was poured into poly(acrylonitrile-co-butadiene-co-styrene) (ABS) moulds, that were dissolved in acetone after the polymer curing time, freeing parts otherwise inaccessible.

The overall structure presents four chambers separated by a 3mm wall: the two external ones, each of a volume of 75 cm^3, housing the combustion process, and two inner ones, of a volume of 80 cm^3, storing the liquid to be pumped.

Once the external ones are fed with an air-methane mixture

Fig. 13 Heart shaped soft robotic pump.

with slight oxygen excess, a logically-controlled spark starts the combustion process: the stretchable walls then decrease the inner volumes, displacing the liquid.

Although, under significant thermal stress, the overall structure temperature stayed significantly below the 320 °C sustainable by the silicone. Indeed, in the worst case, without cooling system the maximally reached temperature was of 200 °C after prolonged actuation.

Because of its actuation typology, the device, although it's introducing advances in soft pumps and showing good performances with respect to physiological environments conditions, seems unsuitable for TAHs applications.

There are some other devices, instead, that have been presented as tentative alternative to the ventricular assist devices, or total artificial hearts. To date, although promising and farsighted, none of them have reached the minimum physiological conditions required, so further improvements will be needed.

2.2.1 Soft Assistive Devices

The device, resembling to a sleeve developed by Walsh at al., shown in Fig. 14, is tentative assist device, since it has been shown able to support the cardiac pumping functionality of a failing heart [27, 28, 29]. Once implanted, it surrounds the heart muscle, and, by being actuated pneumatically, it develops a compression force to strengthen the expulsion of the blood from the natural, but damaged, ventricle.

The simple, but smart, structure aims to replicate the stratified nature of the myocardium, proposing two layers of differently oriented McKibben actuators, embedded into a polymeric matrix. Upon inflation the soft elements contract and generate a cardiac-like motion: constituted by both compression and twist.

The tested devices proposed two different stratification options and two polymer layer thicknesses.

To improve contraction quality, the two layers of actuators, were disposed circumferentially, for contraction, and helically, inclined with an angle of 60 ° with respect to the basal plane, for twisting. In the first proposed disposition the circumferential layer was positioned outside, while the second one it was inside. A higher volumetric displacement was achieved when the twisting actuator was positioned externally, thus this was the preferred configuration for later trials. It is important to

Fig. 14 Soft robotic assist sleeve

notice that the simple activation of one layer (circumferential or twisting), instead of the combined one, showed worse performances.

Then, two thicknesses of the polymeric structure were tested, 15 mm, 550 μm respectively. The second one showed better performances, since the actuators were not limited by the material when moving.

The device was tested both in vitro with univentricular mock circulation loops, and in vivo in porcine models. The ability to activate the different layers separately, and eventually to turn off the device in case of restored contraction, guaranteed the ability to sustain and restore the failing ventricular pumping functionality.

2.2.2 Soft Total Artificial Hearts

For what concerns the soft version of the TAHs, two are the devices that need to be mentioned and in deep presented.

2.2.2.1   McMurray, poroelastic foam sTAH

The first one is an inflatable, polymer-made porous structure that, after being inflated, modifies the internal volume of its chambers, to eject the fluid from the artificial ventricles. Shown in Fig.15.

The device [30] presents four valves, two are responsible of the airflow control, while the other two of the alternation of pumping states between the ventricles.

When A1 is open, the inflation of the left chamber starts, and A2 is venting. At the same time W1 is open to leave open the passage to the right ventricle of the fluid contained in the pressurized adjacent chamber. W2 is then opened and a microcontroller switches the device to the opposite state, starting the inflation of the right chamber.
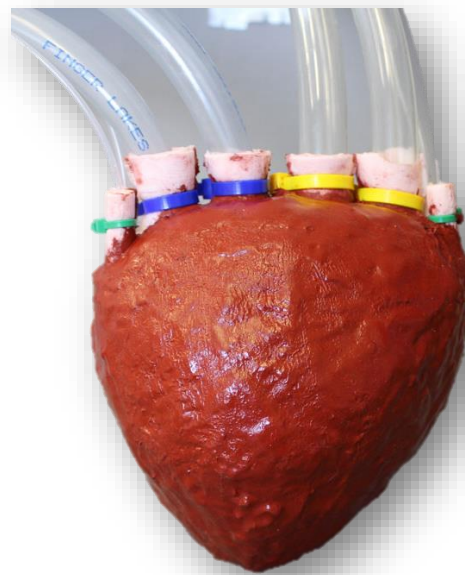
Fig. 15 Poroelastic foam based soft heart

The output flow at frequencies of 2, 1, and 0.1 Hz was measured, and rates of 190 mLmin^{-1}, 370 mLmin^{-1}, and 430 mLmin^{-1} at pressures of 20, 14, and 12 kPa, respectively, were obtained. Although the last one is the fastest flow rate obtained by any other previously reported soft pump [31], it is clear that it is not enough to guarantee a sufficient flow if employed as a TAH.

2.2.2.2   ETH, Silicone sTAH

The same problem is reported by another soft pump, this one developed by a group of ETH engineers [32]. The device, shown in Fig.16, is a 3D printed heart-shaped pump, obtained with the lost-wax casting process.   Externally,   it   presents   the   same dimensions and shape of a human heart; while internally, it is composed by three

chambers, two acting as ventricles, while the other one, positioned between them, develops the ejecting force once inflated.

The reported flow rate was measured by employing a hybrid mock circulation under different physiological conditions. The sTAH achieved a blood flow of 2.2 L/min against a systemic vascular resistance of 1.11 mm Hg s/mL (afterload), when operated at 80 bpm. At the same time, the mean pulmonary venous pressure (preload) was fixed at 10 mm Hg. An aortic pulse and mean pressure of 35 mmHg and 48 mmHg, respectively, were measured.

Fig. 16 3D printed soft artificial heart

In this case, apart from the insufficient output flow, also another was presented. The device, indeed, because of its shape, had a life of at maximum a 3000 working-cycles, i.e. the beating functionality lasted about 30 minutes.

So, although farsighted and promising, these works were not able to find a concrete alternative solution to the already present ones.

3 Concept

3.1 Introduction to Soft Robotics

The aim of this work is to study a novel typology of a bioinspired soft actuated total artificial heart. To this purpose an introduction on the available soft robotics technologies is mandatory.

For years, in the collective imaginary, robotics has been linked to the idea of dangerous industrial machines, bulky service robotics or scary humanoid robots.

Lately, however, a completely different typology of robots made its way through the already commonly known ones. These new intelligent devices presented completely different characteristics: usually highly bioinspired, able to replicate closely the animals' motions, almost uncapable of harming the user, often easily reconfigured thanks to their modular structure, and, even more surprisingly, made of soft materials.

One of the first robots, belonging to this new robotics field, was the one presented by Cianchetti et al. [33], aiming to replicate as close as possible the motion of an octopus arm. Bioinspired, soft and modular: this robot was able to achieve motions that beforehand, without the employment of soft materials, were unthinkable. It is trivial to say that the traditional notion of finite degrees of freedom, since often theoretically infinite, as in an octopus arm, was overtaken by the idea of "a number of" multimodal deformations.

While enlarging, on one side, the range of achievable motions, this redefinition caused complications in control techniques, making up a completely unexplored, yet incredibly interesting, research topic in this field, too.

To be able to produce and control structures, completely or partially deforming as continuous matters, it became important to study and develop intelligent materials, whose behaviour would influence simultaneously both the actuation and the sensing systems.

Focusing more in detail on the actuation, the currently employed technologies can be classified either by typology of the actuated matter, i.e. active, passive or semi-active,

or by material activation principle, electric, magnetic, fluidic, i.e. hydraulic or pneumatic, or other, as optical or thermal. In Tab.1 the so far used technologies are summarized.

Shape-Memory Alloys (SMA), for example, have the intrinsic capability to recover their original shape by being heated over a certain temperature threshold. Lightweight, remotely controllable, employing low voltages, they also allow the miniaturization of the devices, because of these advantages, they were used in different works [34, 35]. On the other hand, however, to be efficiently used, they need relatively high currents, and, because of their high non-linearity and hysteresis can be difficult to control. Similarly, the Shape-Memory Polymers (SMP) have the ability to recover an initial state after deformation; however, they differ in the typology of external stimuli. In this case light, magnetic field, chemical reactions or temperature variation can activate the process. The drawback is that the response time can be very long.

Electro-Active Polymers are another class of actuators that are gaining attention because of their capability to emulate deformations, elasticity, hardness and stiffness of the natural muscles. Generally, they are able to change shape and size when electrically triggered [36]. Their usage is usually limited by the fact that they need high voltages and fields to work efficiently, making them unsuitable also for the artificial organs field.

Flexible-Fluidic Actuators (FFA) are soft-bodied actuators that can be pneumatically or hydraulically driven and their final motion is determined mostly by their shape. Indeed, by exploiting external/internal patterns, coupling different materials or constraining the motion with external braided sleeves as in the case of the Pneumatic Artificial Muscles (PAMs), they can bend, elongate, twist or contract. They are generally lightweight, reliable, flexible, low cost and exhibit high power densities. [37]

Cable-driven actuation presents the advantage of continuous action obtained by controlling cables driven by motors, that can be placed in a remote place. They offer low inertia, weight, and volume, and guarantee a long-range transmission of force and power. However, they present the disadvantages of having just a global action and the necessity of sleeves and/or pulleys to propagate the motion. [38]

In the same field, also jamming technologies gained attention. Depending on the jammed matter, they can be classified as granular, e.g. coffee, rice, sugar, or fibre, e.g. different materials threads, or layer, e.g. paper sheets.

Tab. 1 Soft robotics technological solutions for actuation purposes

Technology	Short Name	Material Typology	Activation Principle	Power Source	Pros	Cons
Shape Memory Alloys	SMA	Active	Thermal	Electrical	Weight, voltages, dimensions	Currents, hysteresis, non-linearities, temperatures
Shape Memory Polymers	SMP	Active	Thermal	Optical, Magnetic, Chemical, Thermal	"	Long response time
Electro-Active Polymers	EAP	Active	Electrical	Electrical	Muscle-like properties, fast activation	Voltages, fields
Magneto-Rheological Based Actuator	MRM	Semi-Active	Magnetic	Magnetic	Response time	Fields
Electro-Rheological Based Actuator	ERM	Semi-Active	Electrical	Electrical	"	Fields
Flexible Fluidic Actuators	FFA	Semi-Active	Pneumatic, Hydraulic	Pneumatic, Hydraulic	Weight, cost, reliability, power density	Bulky power source
Cables	--	Passive	Mechanical	Mechanical	Weight, inertia, volume	Only global action, pulleys
Jamming (Granular, Fibre, Layer)	--	Passive	Mechanical	Pneumatic	Cost, fabrication	Controllability, volume and weight (granular)

By applying vacuum to a chamber containing these materials, the increase of friction between the particles, fibres or layers, causes a simultaneous increase of the system stiffness. [40]

While the magneto- and electro-rheological based technologies can be used for actuation thanks to the coupling of passive structures with fluids able to actively change in their intrinsic properties characteristics, thus defined semi-active, the jamming ones employ completely passive matters.

All these actuation methods enable the design of intelligent soft bodied robots.

3.2 Embodiment theory and cardiac mechanics

As already mentioned, the importance of smart structures is mandatory in order to achieve bioinspired movements.

In nature, indeed, this concept becomes very clear whenever observing soft bodied animals: the overall disposition of their muscular fibres results to be extremely functional to the movement they are designed for. This concept is one of the most important pillars of the soft and bioinspired robotics, too, and it is known as "embodiment".

The embodiment theory refers to all those properties intrinsically embedded in the body of a designed structure. In particular, its ability to act and respond in a highly functional manner, just relying on its shape, mechanical properties and arrangement, is called embodied intelligence. This property, indeed, enables the body, or the "hardware", of a living or artificial being to perform an important part of the computations, that would be otherwise very complex to achieve just by control, or software, strategies. [41]

For example, the muscular disposition of the fibres in an octopus arm, is naturally designed to enable not only a precise positioning, through bending, torsion, elongation or contraction movements, but also a powerful force generation, through stiffening, resulting from the muscular contraction. Thus, although soft bodied, it is extremely accurate in grasping tasks, and efficient when dealing with locomotion ones. [33]

Consequently, when thinking about a possible bioinspired design for a completely soft total artificial heart, the concept of embodied intelligence naturally gains great importance.

In particular, a detailed insight into the cardiac contraction mechanics revealed that, although studied since centuries ago, the muscular fibres disposition in the heart was unrevealed just some decades ago by a Spanish scientist: Francisco Torrent-Guasp.

Torrent-Guasp was the first one to be able to demonstrate the continuity of the cardiac muscle, and its functional arrangement. [43] Indeed, although it has always been known that the complexity of cardiac cycle mechanics was due to an as much complicated muscular arrangement, nobody ever thought it was generated by a unique band.

This theory, indeed, substituted the previous shell-like or layered structure one, where it was thought that the incredibly efficient composition of contraction, elongation

and twisting motions, was given by the contraction of completely independent and different overlapping muscular layers.

In fact, this belief resulted to be just partly true: the powerful but self-tuned blood ejection is indeed activated by a sequential contraction of a unique cardiac band folded in a double helix.

This may be surprising but, as shown in Fig.17, helices and spirals are quite common and recurrent structures in nature. [43]

They can be found in the harmonic pattern of a fingertip, flowers, animal horns, seashells, but also, at the basis of our lives, in our DNA. In the same way, also the heart presents this pattern: and this becomes extremely clear if one looks at it from the apex [44].

Torrent-Guasp was the first one to be able to dissect the heart unrevealing this fundamental structure. After releasing the strict connections of the connective tissue, by boiling it, and then following the natural inclination of the fibres, he was able to show that it is possible to dissect a heart without the help of any particular tool, other than the use of our hands. The cardiac band can be divided into two loops: one called basal, and the other called
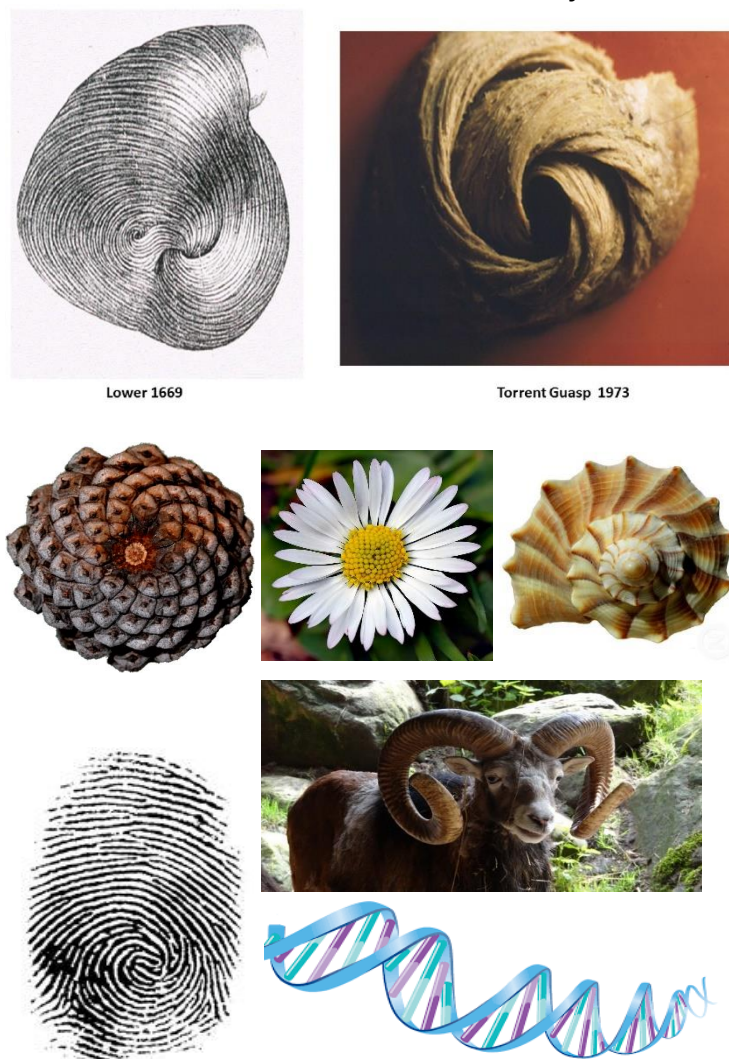

Fig. 17 Helical structures in nature

apical. The first one is generated from the pulmonary artery, surrounds the right ventricular free wall, and creates the first layer around the left ventricular free wall.

From here the apical loop begins, generating first the descending loop (DS): thanks to the higher inclination angle with respect to the basal plane, the fibres form the septum, the wall between the two ventricles. From here, they surround the left ventricular base and create the second layer that covers the left ventricular free wall, i.e. ascending segment (AS), ending at the base of the aorta. The AS fibres cross the DS ones at the septum level, creating a 90 ° angle.

Fig. 18 shows the passages necessary to unravel structure, along with a schematic representation of the fibre disposition.

The muscular arrangement, thus, results in a double layer of myocardium around the left ventricle, generating the previously observed thicker wall, and higher internal forces, with respect to the right ventricular ones.

Moreover, it explains the observed typology of contraction: innovative MRI techniques demonstrated the sequential activation of contraction of the band. Electrical and mechanical contraction, indeed, are correlated but different.

Also, simulations, replicating structures folded in a similar way as the cardiac band, showed that a sequential activation, generates a reduction of the internal volume similar to the ventricular one. [45, 46]

It is clear that the cardiac band is one of the most evident examples of embodied intelligence in nature: the anatomy is fundamental for the final pumping functionality, indeed, just a contraction of 20% of the myofibrils, generates an overall 60% volumetric reduction. [47] Moreover, any of its alterations, as seen in Section 1, brings to dangerous pathologic conditions, as heart failures.

The goal of this work, thus, is to set the basis for a novel bioinspired soft robotic total artificial heart. Two are the main features taken into consideration: 1) the helical arrangement of the cardiac band to be built, 2) its sequential activation during contraction.
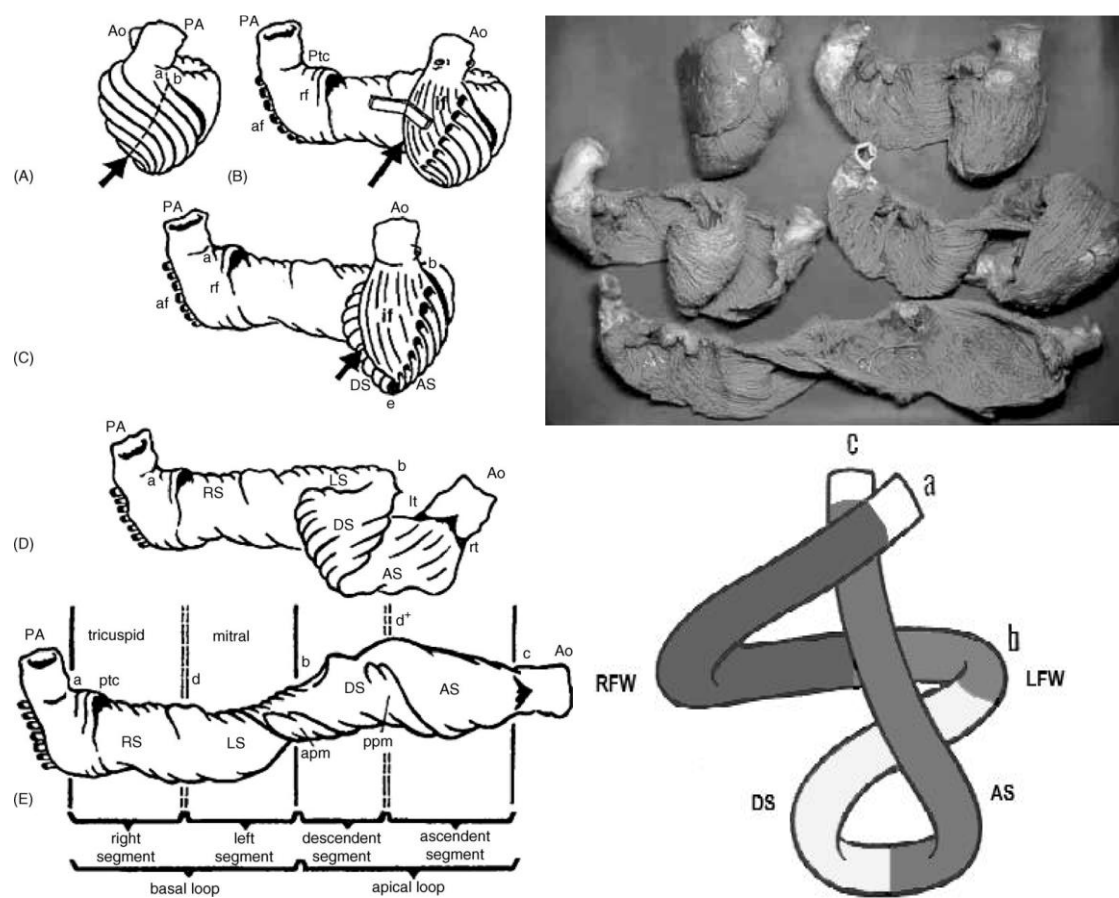
Fig. 18 The helical myocardial band as studied by Francisco Torrent-Guasp

4 Materials and Methods

To be able to set the basis for the development of a total artificial heart, the geometrical model of a tentative left ventricular chamber, along with its muscular arrangement, was designed. Then, in order to simulate the myocardial sequential contraction, the basic actuating unit was chosen.

4.1 Left ventricle geometrical model

Given the importance of the left ventricular pumping functionality, the present study focused on the left ventricular chamber. Indeed, capable of generating higher internal forces, the left ventricle clearly represents the biggest challenge from a design point of view.

As already mentioned, the cardiac anatomic intelligence is the most important pillar on which the whole contraction mechanics is based. For this reason, different studies trying to accurately model the left ventricular shape. [48,49,50]

However, for a sake of simplicity, the first tentative ventricular chamber was modelled as a cylinder, while the myocardial fibres were approximated by actuators, helically wounded around it. Indeed, during the cardiac cycle, the contraction of the myocardial band helix corresponds to an internal volume reduction, thanks to the composition of three movements: an axial contraction, a radial one and a twist.

While the contractions both along the axial and the radial directions help the overall volume reduction, the twist seems to be just a result of the geometrical disposition of the fibres: the momentums affecting the band, in fact, are not geometrically compensated. This results into a clockwise rotation of the base, and an anti-clockwise rotation of the apex during the cardiac cycle, as shown in Fig.19. [51,52]

Even if a certain correlation was observed between the decrease of rotation and torsion angles during the cardiac motion and some pathologic conditions affecting the overall ejection fraction [53], their functionality has not been completely understood yet. For this reason, in the developed model, the overall rotation was blocked.

To date, different the studies tried to model the helically wounded muscular bands effect on the typology of movements achievable by soft bodied animals [54, 55, 56, 57]: however, in literature, there are no works dealing with their effect on hollow structures.

In this work, instead, a first modelling attempt in this direction was made. It was of great interest, in fact, to understand how the contraction of an actuator helically wounded around a certain volume influences its overall volumetric reduction.

Fig. 19 Rotation and torsion diagrams of the base and the apex during the cardiac cycle

Related to this, it can be interesting to mention that in the cardiac mechanics, to a myofibrillar shortening corresponds also to a thickening, and thus to an inner section reduction. Moreover, thanks to this functional arrangement and characteristics, a 15-20% muscular fibre contraction is sufficient to produce a 60-70% internal volume reduction. [58]

The model was thus based on a) some basic geometric hypotheses, defining the initial and final state, and on b) other imposed conditions, that guaranteed a system deformation similar to the just explained physiological one.

For what concerns the geometrical hypotheses, they give information about the overall system: the ventricular chamber is modelled as a cylinder, while the helically wounded muscular band, is represented by a one-dimensional actuator, wrapped around the walls of the cylinder.

Then, to completely characterize the typology of deformation during the contracting phase, the following assumptions were added: a) the helix angle θ constant and equal to 54.7 °, b) constant number of turns, and c) constant ventricular walls overall volume.

The above listed hypotheses lead to a contraction similar to the one showed in Fig. 20: a shortening of the actuator causes a redistribution of the cylinder walls volume.

Fig. 20 Modelled ventricular contraction: the shortening of the

L – Helically wounded actuator length

H – Cylinder height

C – External circumference multiplied by the number of helix turns

θ – Helix angle
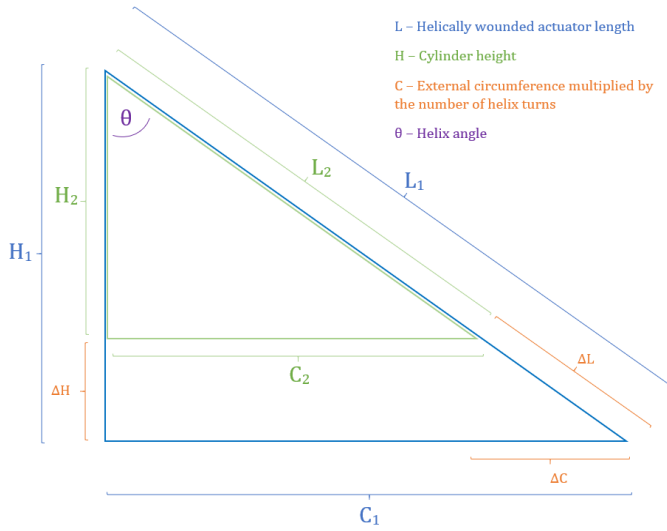
Fig. 21 Unrolled view of the helically wounded actuator: contracted (green triangle) and relaxed (blue triangle) state parameters are shown.

To a shortening along the axial direction corresponds an increase of walls thickness, thus a cross-sectional necking.

The equations, on which the model results are based, were obtained from considerations on the planar development of the helically wrapped actuator, as shown in Fig. 21.

The parameters are H, the height of the cylindrical chamber, C, the external circumference multiplied by the number of turns n, and L the actuator length.

The blue triangle represents the relaxed condition, while the green triangle the contracted one. By applying the model hypotheses these are the resulting equations:

$$\begin{cases} H = L\cos\theta \\ C = L\sin\theta \\ n = \dfrac{C}{2\pi R_{out}} \end{cases} \quad \wedge \quad \begin{cases} V_C = \pi(R_{out}^2 - R_{in}^2)H \\ V_b = \pi R_{in}^2 H \end{cases}$$

$$\begin{cases} \dfrac{H_1}{L_1} = \dfrac{H_2}{L_2} \\[2mm] \dfrac{C_1}{R_{out1}} = \dfrac{C_2}{R_{out2}} \\[2mm] \dfrac{H_1}{H_2} = \dfrac{R_{out2}^2 - R_{in2}^2}{R_{out1}^2 - R_{in1}^2} \end{cases}$$

Where n is the number of turns, R_{out} and R_{in} are the outer and inner diameter, V_c the cylinder walls volume and V_b the internal volume, corresponding to the volume of blood contained in it. The subscript 1 indicates the initial relaxed phase, while 2, represents the final contracted phase. The geometric parameters of the chamber at the initial state were set to match the average physiological ones, typical of the end-systolic (ES) condition.

The main aim of this model was to determine the amount of shortening ΔL of the helically wounded actuator, needed to achieve a physiologically acceptable ejected blood volume ΔV, to equal the average stroke volume (SV). These parameters were defined as:

$$\Delta L = L_1 - L_2 \qquad \wedge \qquad \Delta V_b = V_{b1} - V_{b2}$$

4.2 Experimental Validation Setup

To validate the model an experimental setup was built. First, a physical model of the simplified ventricular chamber was fabricated. To reduce the resistance of the material to the compressing action of the actuator, a silicone with low elastic modulus was chosen (ECOFLEX™ 00-30, SMOOTH-ON! Inc).

The mixture was then poured, degassed and let to cure inside an assembled mould. The mould, as shown in Fig. 22. is composed of four concentric plexiglass discs, connected through supports, obtained through laser-cutting techniques.

The lateral surfaces, then, were obtained by adapting PVC transparent sheets to the mould. The silicone was poured inside it through four holes cut on the top disc, and, once it was completely cured, two thin layers, 2 mm, of the same material were made to secure
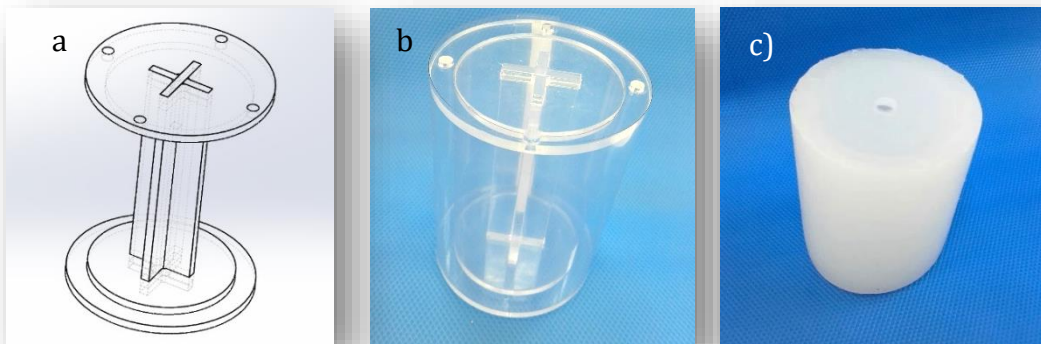
Fig. 22 Fabrication of the cylindrical chamber, as in model: a) CAD model of the mould, b) final assembled mould and c) final ECOFLEX 00-30 casted chamber.

the chamber. An 8 mm hole was left on top of the chamber, in order to be able to fill it with water and connect it to a graduate cylinder for volume displacement evaluation.

Two couples of four, commercially available, braided sleeves were mounted onto the cylinder. Successively, nylon cables were run through the sleeves: this helped to reduce the friction between the ECOFLEX™ 00-30 chamber and the actuator itself, while simultaneously guiding its motion along the predetermined helix angle θ of 54.7 °.

Indeed, it was computed that by maintaining this angle during the motion, the shortening of a couple of antagonistically mounted helical actuators, results into the most efficient volumetric contraction.

In order to prevent the downward motion of the silicone base of the cylinder, due to the weight of the water, and to block, at the same time the position at one end of the actuators, a plexiglass base was mounted, after being treated with some silicone oil, to reduce friction.

Finally, to be able to pull simultaneously and vertically all the cables, a plexiglass structure was built and fixed to a tensile-compression testing machine (INSTRON 4464). This structure, as shown in Fig. 23, helped to maintain the cylinder in position while puling the nylon wires.

The shortening obtained through the model was imposed on the machine, and the ejected volume was evaluated by observing the amount of water displaced inside a graduated cylinder at the end of the contraction. The final experimental setup is shown in Fig. 23.

Fig. 23 a) Final experimental setup and b) zoomed view on the tested physical model

4.3 Actuator Choice

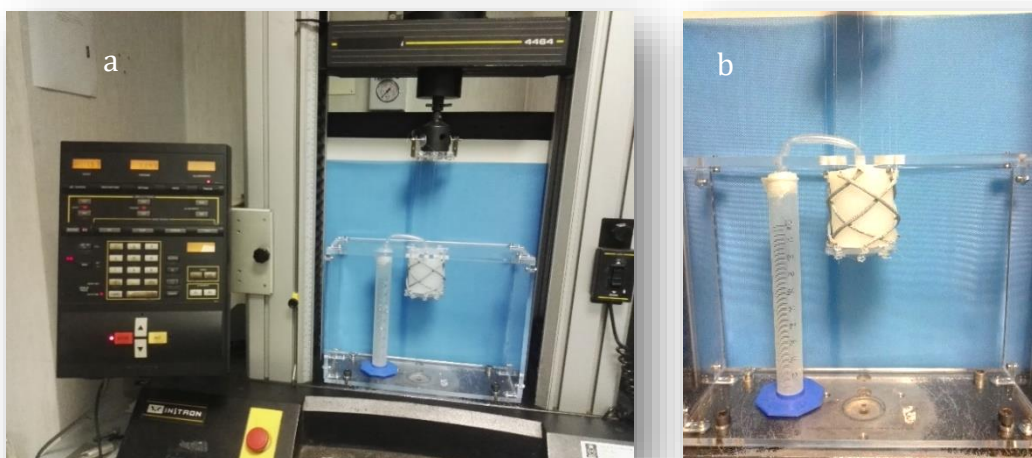At this point of the work, in order to be consistent both with the requirements imposed by the physiology and the considerations deriving from the geometrical model, the fundamental characteristics of the single actuating unit were summarized as follows:

a) muscle-like shortening: a sarcomere contracts of an average 20%

b) the possibility to be activated sequentially: to reproduce the cardiac mechanics

c) thickening, i.e. radial expansion, to contribute to the cross-sectional decrease of the ventricular chamber

d) possibility to be miniaturized, to increase the actuated surface of the chamber walls without increasing the overall dimensions

e) present limited or no risks for health in case of implantability.

All these requirements seemed to be satisfied by a specific kind of flexible fluid actuator, well known for its muscle-like performances: the McKibben actuator, a pneumatic artificial muscle (PAM).

4.3.1 The Pneumatic Artificial Muscle

The pneumatic artificial muscles, are a group of actuators, belonging to the FFA class. They were invented in the late 50s, and first commercialized in the 1980s by the Bridgestone rubber company (Japan): their first application was in the artificial limbs area.

The PAMs are pneumatically actuated, and they are generally composed of an internal expansible elastomeric bladder, surrounded by an outer braided mesh, responsible of constraining the expansion into a specific deformation. [59]

If flexible fluidic actuators can produce, by exploiting the similar principles, motions as torsion, and bending, these muscles are generally specialized in contraction movements [37].

Light-weight, low cost, capable of high forces, not presenting risks for the human health, and known for their capability to approximate muscular behaviour, they seemed to be the best choice as basic actuating unit.

As in Fig. 24, the working principle is very simple: upon pressurization, the bladder tends to expand both radially and axially because of its elastomeric nature. However, the tensile strength of the threads composing the outer braided sleeve, constrains the elongation, leading to an overall system axial contraction, and a simultaneous radial expansion.
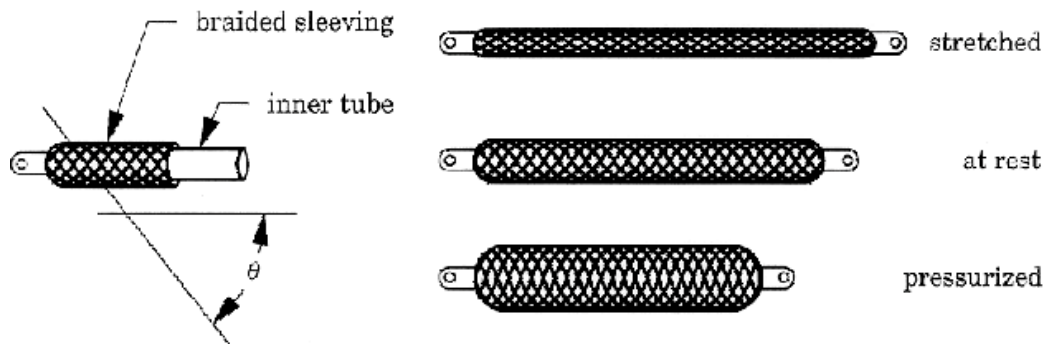
Fig. 24 Basic representation of the McKibben muscle working principle

4.3.2 McKibben Muscle geometrical model

Different attempts were made to model the McKibben actuator behaviour. Although, the working principle is simple, the number of parameters playing a role, especially when trying to model the muscle in dynamic conditions, is large.

In general, the aim of the presented models was to predict the amount of shortening upon pressurization, that causes an inner volumetric change.

Considering for simplicity static conditions, one can approximate the behaviour of the actuator, just by considering its geometry.

The parameters that need to be taken into account are both depending on the braided sleeve and on the chamber dimensions. Shown in Fig. 25, they can be listed as follows: a) braided sleeve length, b) braiding angle, c) chamber length, d) chamber

diameter. [60] The chamber and braided sleeve length can be approximated to the overall actuator length.
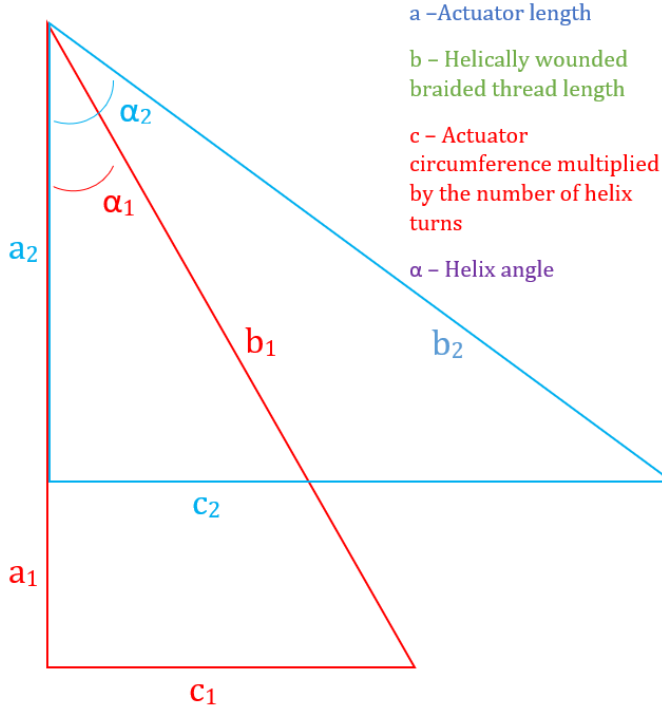
Fig. 25 Geometrical model of a McKibben pneumatic artificial muscle. Relaxed (red triangle) and pressurized (blue triangle) state parameters are shown

Then, the main geometric assumptions can be summarized as follows: a) braided sleeve thread of constant length, b) cylindrical inner volume c) negligible bladder wall thickness.

In Fig.25, the red triangle represents the relaxed condition, while the blue triangle the contracted one. The system can be described by the following equations:

$$\begin{cases} a = bcos\alpha \\ r_{mck} = \dfrac{bsin\alpha}{2\pi n} \\ V = \dfrac{b^3 cos\alpha \sin^2 \alpha}{4n^2\pi} \end{cases}$$

Where, a is the actuator length, b the constant thread length, α the helix angle, n the number of turns of the helically wounded thread, V the inner volume. In static conditions then, by applying the virtual work principle, it is possible to determine the developed force of the actuator:

$$F = -P_2 \frac{dV}{da} = \frac{P_2 b^2 (3\cos^2 \alpha - 1)}{4n^2\pi}$$

Where F is the obtained force, and P is the applied pressure.

In dynamic conditions instead, additional parameters should be taken into consideration, e.g. friction between overlapping threads, friction between the bladder and the external mesh, hysteretic behaviour of the elastomeric material, chamber walls thickness, etc. [61,62]

4.3.3 Fabrication and testing

Following the model guidelines different actuators were fabricated and tested, Fig. 26. Tab.2 summarizes briefly the different materials that were employed. They were tested mainly in terms of contraction ratio, defined as:

$$\varepsilon = \frac{l_i - l_f}{l_i}$$

Where l_i corresponds to the initial length, and l_f to the final one. Fig.26 shows some of these fabricated and tested actuators.

Fig. 26 Example some of the fabricated and tested actuators. From top left actuator 1, 2, 3a, 3b, 3c, 3d, 5, 6, 7

Tab. 3 and Tab. 4, instead, summarize more in detail, the characteristics of the actuator that was chosen as most suitable, both in terms of employed chamber and sleeve. In particular, the chosen chamber material was preferred to the already commercially available ones since the casting process gave the opportunity to tune not only the thickness of the walls, making it more resistant, but also the elastic modulus of the camber, determining the typology of expansion. For what concerns the sleeve material, instead, PVC was the selected one because of its tensile strength, in general allowing better contraction ratios, but also ease in fabrication and reproducibility, characteristics that other tested sleeves did not present, e.g. paper or cotton thread.

Thus, as just mentioned, the preferred fabrication methods were: casting for what concerns the internal chamber, and thermoforming for the braided sleeve that was already commercially available. This last process allowed to decrease the braiding angle

and the diameter of the mesh, improving its performances when coupled with the elastomeric chamber. To the same purpose, also some threads were removed, this helped the braid angle deformation during the motion.

To be able to obtain a bladder with the designed specifications, a mould was manufactured with a 3D printing lost-wax process. The obtained mould is shown in Fig. 27.

Once completely cured, the chamber was extracted and run through the modified braided sleeve. Then, as it can be observed in Fig. 28 one end was used as supply pressure inlet port, while the other one was secured, to prevent air leakage.

To test the actuators, a setup was built, the actuator was connected in series with a digital manometer, CAMOZZI SWCN-P10-P3-2, to measure the pressure, and finally, some graph paper was used to quantify the overall actuator shortening.

Tab. 2 Tested actuators chamber and sleeve materials.

ACTUATOR NUMBER	CHAMBER MATERIALS	SLEEVE MATERIALS
1a-b	Commercially available silicone tubing	Commercially available Farnell, PVC, Dout=3 mm
2	Commercially available silicone tubing	Commercially available Farnell, PVC, Dout=3 mm
3a-c	Casted Ecoflex™ 00-30, SMOOTH-ON Inc.	Commercially available Farnell, PVC, Dout=5 mm
3d	Casted Ecoflex™ 00-30, SMOOTH-ON Inc.	Commercially available Farnell, PVC, Dout=4 mm
4	Casted Ecoflex™ 00-30, SMOOTH-ON Inc.	Commercially available Farnel, PVC, Dout=5 mm
5	Casted Ecoflex™ 00-30, SMOOTH-ON Inc.	Laser-cutted Cellulose polyester paper
6	Casted Ecoflex™ 00-30, SMOOTH-ON Inc.	Commericially available Uniaxially stretchable textile
7a-b	Casted Ecoflex™ 00-30, SMOOTH-ON Inc.	Hand-braided cotton wire
8	Commercially available latex tubing	Commercially available Farnell Dout=5 mm

Tab. 3 Internal elastomeric chamber properties and dimensions

PARAMETER	VALUE
Chamber material	ECOFLEX 00-30
Wall thickness s	1 mm
Length a	55 mm
Initial outer diameter D_{out}	5 mm

Tab. 4 External sleeve properties and dimensions

PARAMETER	VALUE
Sleeve material	PVC
Braiding angle α	25 °
Length a	60 mm
Initial outer diameter D_{out}	4 mm
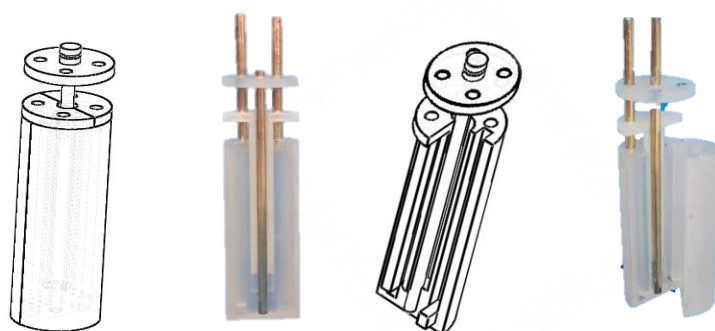
Fig. 27 Single actuator chamber 3D printed mould: CAD and obtained models.
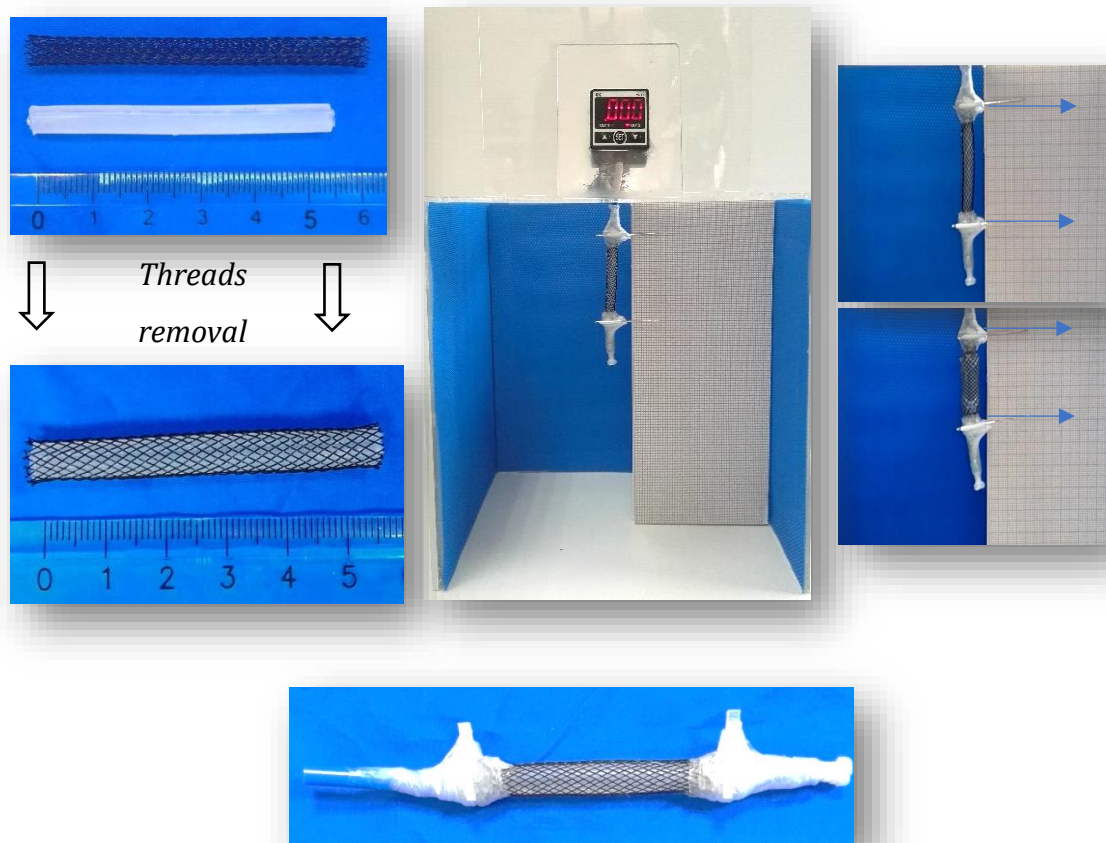
Fig. 28 Fabrication and testing of the single McKibben actuator

4.4 Sequential activation

Once the single actuator was chosen, some considerations about the possibility of a sequential activation of the different muscles were advanced.

Indeed, another important characteristic of the helical ventricular band underlined by the studies of Torrent-Guasp, is the myocardial mechanical sequential activation, which does not correspond to the path, followed by the electrical signal.

As a very first explorative approach, in order to be able to activate sequentially different McKibben muscles, connected in series, the design of a smart, but completely passive connective element, was thought.

This connective element should meet the following requirements: a) be soft, so that the overall series of actuator could be folded into a double helix, b) have a smaller inner

diameter, so that by causing a local pressure loss it would slow down the air propagation velocity inside the series, c) be easily couplable with the actuators chamber.

As a tentative solution, two different silicone connective elements were produced: one made of ECOFLEX™ 00-30, SMOOTH-ON! Inc. while the other one of ECOFLEX™ 00-50, SMOOTH-ON! Inc.. The first one resulted to be too soft: although the internal diameter was of 0.1 mm, it was able to expand and consequently counteract the effect of the actuator shortening. For this reason, the second material was selected, and, to produce a higher number of actuators and connectors simultaneously, a new 3D printed mould, shown in Fig. 29 was fabricated.

This new mould allows to cast two different types of chambers, one with a 3 mm internal diameter, while the other one of a 0.1 mm. The series were then assembled by alternating a McKibben bladder with a connection, gluing them together, with the Sil-Poxy™, SMOOTH-ON!Inc. silicone glue.

Once the chambers were connected, they were run through the braided sleeves, finally secured by the same silicone glue. Fig, 29 shows the process. Finally, as it was done for the single actuating unit, one end was prepared to be used as air supply inlet port, while the other one was secured, to prevent air leakage.

At this point, some geometrical considerations about the possibility to merge the two previously explained models were made. Indeed, if one thinks to split the modelled chamber, along the vertical axis, so that the helically wounded actuator length, corresponds exactly to the McKibben actuator length, the system could be represented as in Fig. 31.
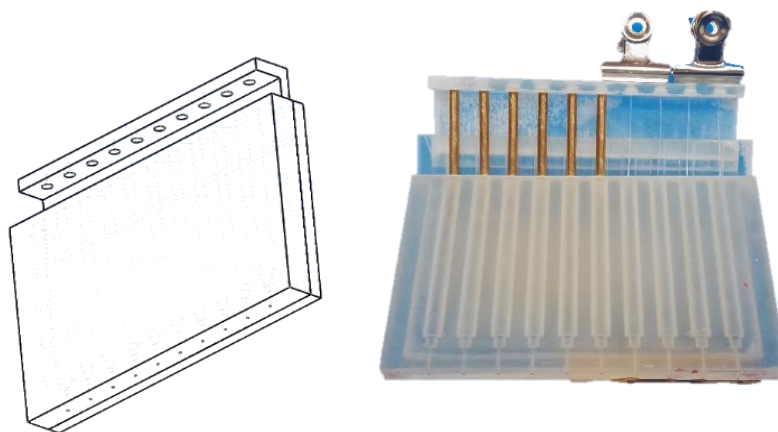
Fig. 29 Multiple actuators and connections fabrication mould

Fig. 30 Fabrication process of the series of McKibben actuators, sequentially activating: a) schematic view, b) chambers and connections assembly after applying the silicone glue c) final series, obtained by securing the braided sleeve around the elastomeric chambers

At this point it is immediate to notice that the chamber and the actuator geometry can be described with the same system of equation just by imposing that at all time instants:
$$L = a$$

Where L and a are the actuator lengths in both models.

L – Helically wounded actuator length

H – Cylinder height

C – External circumference multiplied by the number of helix turns

θ – Helix angle

a – Actuator length

b – Helically wounded braided thread length

c – Actuator circumference multiplied by the number of helix turns

α – Helix angle

Fig. 31 Overall system geometrical model: linking chamber and actuator geometrical models

5   Results and Discussion

5.1 Left ventricle geometrical model

In the following tables, all the model parameters of the initial and final conditions, are summarized. It is possible to see that they are also subdivided between constant or variable values and between computed and fixed ones. A parameter was considered constant if its value was not allowed to change during the motion, while computed whenever it was part of the equation-derived parameters.

Tab. 5 Initial state parameters

INITIAL STATE	CONSTANT	VARIABLE	FIXED	COMPUTED
Initial Blood Volume V_{b1}		X	137 ml	--
Initial chamber height H_1		X	70 mm	--
Initial outer radius R_{out1}		X	32 ml	--
Initial inner radius R_{in1}		X	25 ml	--
Initial actuator length L_1		X	--	121 mm
Number of turns n	X		--	0.5
Cylinder walls volume V_c	X		--	87 cm^3
Helix angle θ	X		54.7 °	--

Tab. 6 Final state parameters

FINAL STATE	CONSTANT	VARIABLE	FIXED	COMPUTED
Final blood Volume V_{b2}		X	43 ml	--
Final chamber height H_2		X	--	58 mm
Final outer radius R_{out2}		X	--	27 mm
Final inner radius R_{in2}		X	--	15 mm
Final actuator length L_2		X	--	101 mm

All the parameters marked as fixed, were imposed by the physiology. This helped a better comparison with the natural ventricular pumping functionality.

Comparing the values referring to the helix length in Tab.5 and Tab.6, it is evident that the model is suggesting a 20 mm shortening of the actuators, to obtain a volumetric displacement of 94 ml.

5.2 Experimental Validation

The goal of the experimental validation was to prove with the fabricated physical model, that the computed shortening was displacing the expected amount of volume. However, the observed quantity of water contained in the graduated cylinder at the end of the experimental trials, was far from the predicted one: an average of 34 ml.

Although, this result prevented the model from being completely validated, it allowed the formulation of some significant considerations about the most suitable actuation technology to be chosen and the ventricular shape importance.

Indeed, the main reason behind such a low ejection fraction, is the fact that the predicted cross-sectional necking is higher than the experimentally observed one. This could be correlated to the fact that our physical model, presents an extremely low ratio between active and passive material.

The myocardium in fact, is composed by 70% of active muscular fibres, while just a 30% of passive connective tissue. In our case, instead, the cylinder walls were completely passive. So, by taking inspiration from the nature, two improvements could have been made: a) choosing an actuator that could become part of the physical model walls, helping the necking process by thickening b) extending the active surface, so that it would be possible to reduce the losses due to the outward motion of the unactuated material.

This adds two important requirements to the envisioned bioinspired actuation system: a) the ability to expand radially while shortening, exactly as it happens with a natural sarcomere, b) the possibility to be miniaturized, so that the highest amount of active surface would be produced, without increasing too much the overall dimensions of the system.

Finally, another remark can be added to the discussion of this result. Although low, and explainable with the abovementioned considerations, the experimentally obtained stroke volume, could have been predicted, just by observing, once again, the performances of a natural cardiac cycle.

In fact, an ejection fraction around 30%, as it is in our case, has been pointed out to be typical of an infarcted heart, that generally presents a dilated ventricular chamber. As already explained in Chapter 1, all cardiac pathologic conditions, bring to the modification of the ventricular chamber shape, making it generally more similar to a cylinder than it would be in healthy conditions, when the EF is around 60-70% of the initial amount. [50]

This observation, thus, should be taken into account when designing a new, and more functional, ventricular chamber shape.

5.3 The McKibben muscles

From the above considerations, merged with the physiological ones, the actuator chosen to be the basic contractile unit was the McKibben pneumatic muscle.

To better understand its performances, and maybe link them to the chamber design, its geometrical model was considered.

Although simple, this model gives important indications about the geometry of the basic actuating unit. It is, indeed, possible to make the following design considerations: a) a low helix angle produces a higher contraction ratio, since the working range is larger, b) the maximum volume is obtained at a corresponding helix angle of 54.7 °, c) the maximum developed force is obtained at the relaxed length, d) the model is the most accurate with thin walled bladders.

Following these guidelines, different actuators were fabricated and compared in terms of shortening mostly. The table below, Tab 7, shows the main performances observed. Actuator 3d) seemed to show the best contraction ratio, thus it was slightly modified and successively tested.

ACTUATOR NUMBER	D_{in}-D_{out} [mm]	THICKNESS t [mm]	BRAID ANGLE α [°]	L_i-L_f [mm]	ε%	THREADS
1a	1.30-1.80	0.25	20	40-34	15	1
1b	1.30-1.80	0.25	20	35-30	14	1
2	1.50-1.80	0.15	20	35-32	8	1
3a	3.00-5.00	1.00	30	45-40	11	3
3b	3.00-5.00	1.00	30	37-30	19	1
3c	3.00-5.00	1.00	30	35-28	20	1
3d	3.00-5.00	1.00	25	35-25	29	1
4	3.00-7.00	2.00	30	40-35	13	1
5	3.00-5.00	1.00	0	40-36	10	/
6	3.00-5.00	1.00	/	35-27	23	/
7a	3.00-5.40	1.20	~25	22-18	18	1
7b	3.00-5.40	1.20	~25	31-26	15	1
8	4.80-5.00	0.40	30	40-32	20	1

Then, the results of the testing procedure of actuator 3d) are summarized in Tab. 8.

Tab. 8 Actuator testing results

	P_{max} [bar]	L_{in} [mm]	L_{fin} [mm]	ε_{max}%
Actuator 1	1.20	52	39	27
Actuator 2	1.48	53	40	24
Actuator 3	1.90	50	35	30
Actuator 4	1.35	48	38	26
Actuator 5	1.12	48	38	20
Average	1.41±0.39	50±2.5	38±2.5	25±5

From Tab. 8 it is possible to observe that the shortening values obtained, are also consistent with the expected performances of the single active contracting unit.

5.4 Sequential activation

Although the sequential activation was not analysed in detail quantitatively, it was possible to make some preliminary observations about the qualitative final contraction.

In fact, just by designing a connective element, characterized by a significant internal cross-sectional reduction, it was possible to achieve a sequential activation of the series of muscles, as shows Fig. 32.

The overall shortening time interval, was much larger than the physiological one, but this mainly depends on the main design parameters of the chamber and of the connective elements. However, this solution showed that it could be possible to replicate the sequential activation of the artificial cardiac band, just by employing smartly designed passive elements, as it actually is in nature, e.g. intercalated discs Chapter 1.

Moreover, by studying this configuration, made by a certain number of identical pneumatic muscles connected in series, it was possible to advance the idea that, because of their similarities, the two geometrical models presented, one for the chamber, the other for the muscle, could be merged into a bigger one.

This could lead to the possibility to control the overall system behaviour, i.e. axial and radial ventricular chamber dimensions, just by managing correctly the input parameters of the artificial muscle.

In particular, the input pressure determines a volumetric change in the actuator that shortens and thickens. These actions influence then the artificial ventricular chamber geometry, causing its subsequent shortening in the axial direction and a simultaneous reduction in the radial one.

So, it is straightforward that, just by measuring one of the geometrical parameters related to the McKibben actuation, it would be possible to determine the overall system condition.
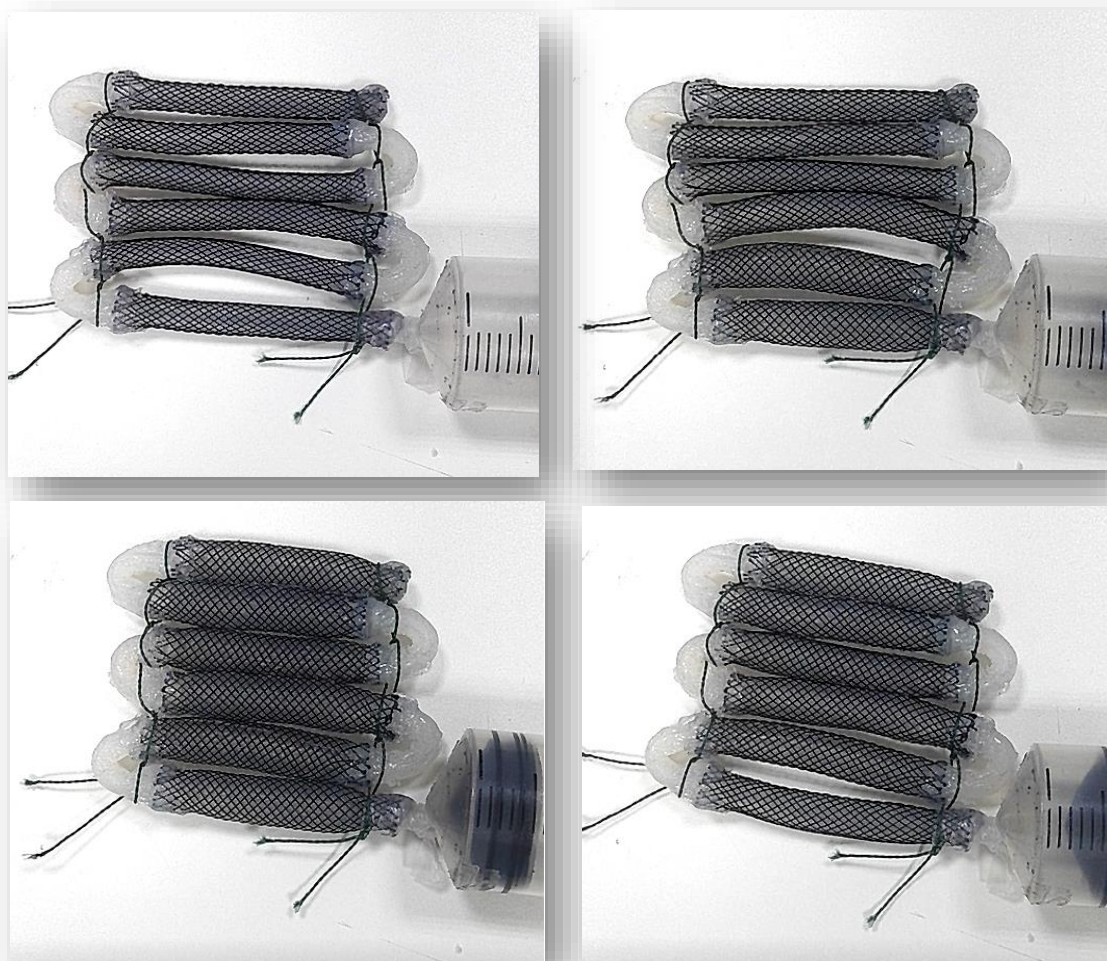
Fig. 32 Sequential activation of the McKibben pneumatic muscles in series

6 Mechatronics design considerations

In the soft robotics field, the control and sensorization of devices is still a hot research topic. Being deformable, stretchable, modular and frequently made of soft materials, these robots are not easy to control. Indeed, as it happens in nature, usually a sensorless but complex and functional actuating structure is preferred to a simple one coupled with intricate control algorithms.

The main difficulty when developing a soft sensor is related to the fact that, besides all the generic requirements a good traditional sensor embeds, i.e. good sensitivity, resolution, accuracy, adequate working range, high signal/noise ratio, no drift, other requirements given by the typology of destination robots must be added. For example, to be able to map the overall system deformation, in complete absence of rigid elements, the sensor itself should be soft, deformable, and/or stretchable, exactly as the structure it needs to sense. In this way, it would not constrain the motion and produce accurate measuring values.

Again, it is clear that the choice of the right material plays a fundamental role. In general, as it is for the traditional sensors, the so far developed technologies can be divided in two groups: a) by the typology of physical quantity measured, b) by operating principle.

For what concerns the first group, the sensors can measure: pressure or force, strain, position, flow, thermal variation, optical characteristic variation, or any type of field, e.g. electrical or magnetic. The measured quantity is strictly correlated to the operating principle too, that defines the following categories of sensors: resistive, capacitive, inductive, electro-magnetic or photoelectrical.

Although, there are different are sensors that were to date employed, this chapter will qualitatively analyse only the ones, that seem to be the most suitable for our purpose.

So far, indeed, both the single actuator and the series were controlled in open-loop, predicting their behaviour on the base of geometrical models. However, it is trivial to say that for such an important application, i.e. a novel type of total artificial heart, even if, in the most optimistic case, where the device will not need active connective elements, and

will be completely able to autoregulate itself autonomously, a feedback on the working conditions of each actuator will be mandatory. By constantly monitoring the actuation parameter it will be possible to promptly treat a failure, or better, even predict it.

In this case, the additional requirements of an appropriate soft sensing system would thus be: a) to be implantable, b) do not present risks for health, c) do not affect the actuation, d) to possibly be embeddable in the actuator itself.

The first solution, could be a device similar to the one presented by Stauffer et al. [63], a soft electronic strain sensor with chipless wireless readout. Designed to provide information about the organs and tissues functionalities, without compromising them, with huge mechanical elasticity mismatch. This soft chipless wireless strain sensor is based on a composite material capable of high cyclic stability. This particular material consists of gold-coated titanium dioxide nanowires embedded in a soft silicone elastomer, while the overall strain sensor is characterized by a stretchable plate capacitor and a coil for inductive readout of its resonance frequency.

The sensor presents the big advantages of being low cost, completely implantable, and based on a wireless transmission, Thus, guaranteeing continuous monitoring. On the other hand, the main disadvantage is the high volume needed for the implantable sensor circuitry, and the better performances linked to large deformations. The final system is shown in Fig.33.
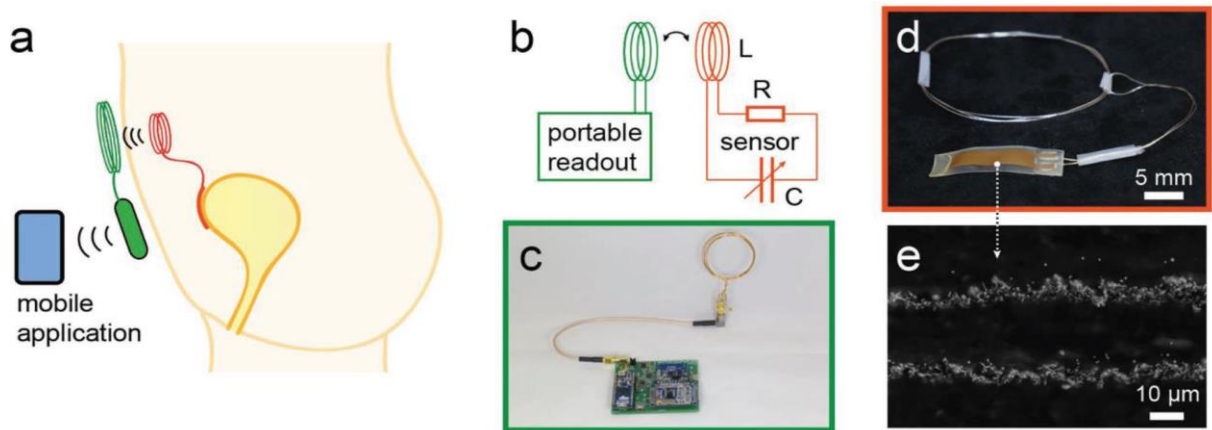

Fig. 33 Soft electronic chipless strain sensor. a) proposed concept, b) circuit diagram, consisting of a RLC circuit where a stretchable capacitor acts as sensing element. the resonance externally is read via inductive coupling c) readout coil d) implantable RLC sensor e) side view of a cut through the stretchable plate capacitor

Another possibility would be to use a smart material as the electrolycra, as proposed in the work of Cianchetti et al. [64] for the sensorization of an octopus arm. The purpose was to evaluate the soft robot position without affecting its performances: the material employed changes conductivity when stretched, allowing to reconstruct the spatial configuration. Although high accuracy, deformability and lightness were reported, this solution would need a high volume of circuitry.

Fig. 34 Sensorization of an octopus arm, and relative configuration reconstruction.

Fig. 34 shows the above described system.

The basic scheme of the sensing system presented by Goulbourne et al. [65], is presented in Fig.35. This study focused specifically on the sensorization of a McKibben muscle by employing a dielectric elastomer in contact with the inner bladder. Once the artificial muscle is pressurized, the bladder and the above-mentioned elastomer deform, allowing the sensing action. This solution presents the big advantage to contribute to the actuation itself, besides being simple to fabricate, present a large strain range, low cost and weight. The only disadvantage is the need of a more accurate geometrical model of the chamber deformation, than the one presented in Chapter 6.

Another solution whose performances were studied on a McKibben actuator, was presented by Hamamoto et al. [66]. By measuring the displacement of a slider on a nylon string coated with carbon, it is possible to measure the performances of the actuator. Indeed, this displacement causes an electrical resistance variation between a fixed electrode and the moving element connected to the inner rubber tube. Fig. 36a depicts the different parts composing the system.

The advantages are the low cost and the accuracy, while the main disadvantage is the presence of rigid elements that might affect the overall actuating system flexibility.
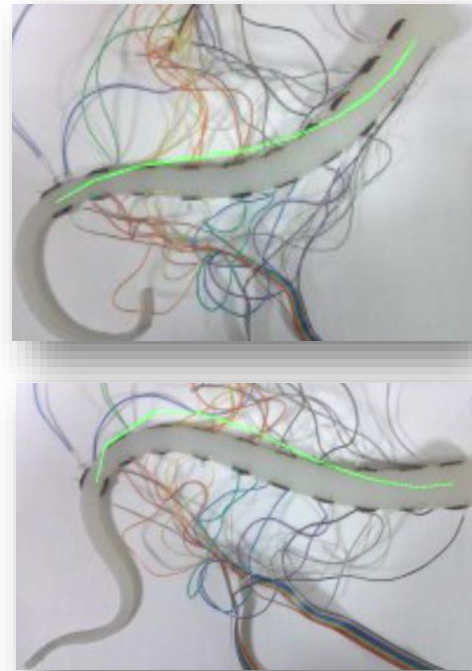
If this system is mostly relying on the measure of the axial length variation, the study of Kuriyama et al. quantifies the radial expansion of the chamber. [67] A flexible conductive rubber sensor is placed circumferentially onto the actuator external diameter. Upon pressurization, the McKibben expands, causing a change in the material resistance. The used material, shown in Fig. 36b, has the advantage of no need of pre-tensioning, as it was in the case of the electrolycra employed for the octopus arm.
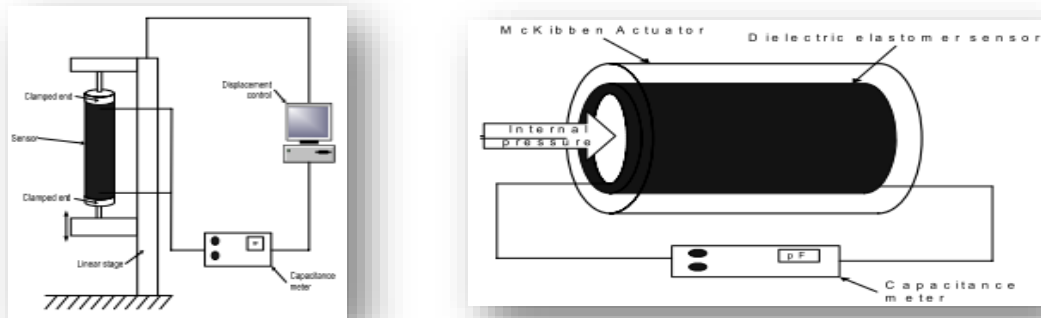

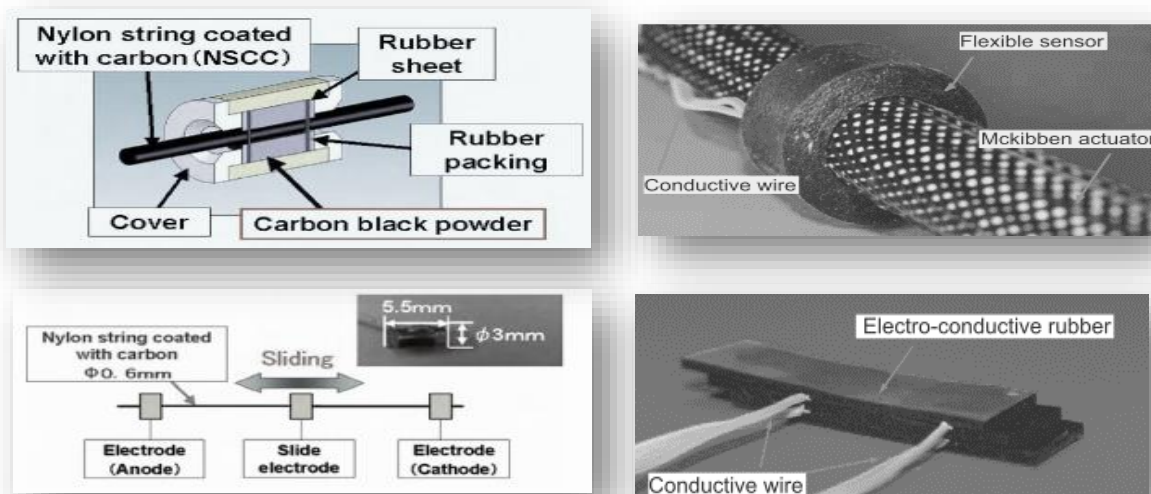*Fig. 35 Dielectric soft elastomer sensor working schematics*

Fig. 36 a) axial displacement sensor mounted on a McKibben muscle, b) radial expansion circumferential sensor

Hirai et al. proposed, for the same application, to measure the torsion of an electroconductive yarn wounded around a polyurethane core, Fig. 37a. When the actuator is pressurized, the yarn changes its number of turns and thus its resistance. [68] Although the solution is not affecting the deformability of the actuator, pre-tensioning is necessary, and the accuracy of the measurement is quite low.

Misumi et al. conducted a study on conductive fibres, in order to substitute them to some of the normal threads constituting the sleeve. The working principle is simple: when the actuator contracts, it expands radially, causing a variation in the electrical resistance of the wires. [69] The system in Fig. 37b is low cost, relying on a simple circuit and it contributes actively to the actuation; however, a very low signal to noise ratio was reported, probably due to the use of only two wires, that necessarily also cross above each other, interfering with the measurement.
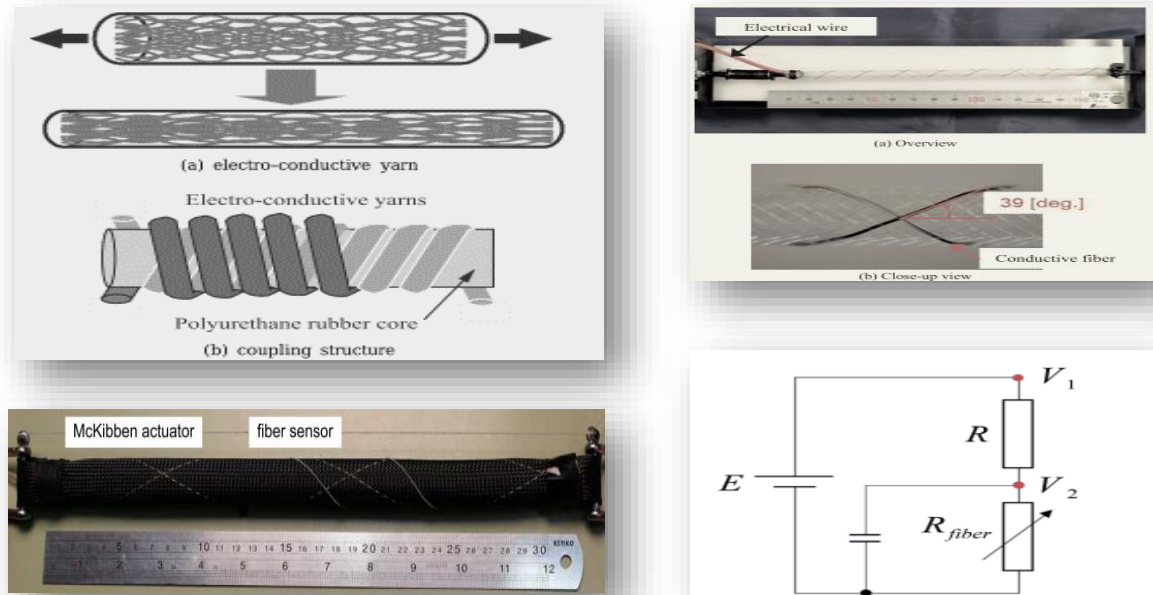

Fig. 37 a) On the left the electroactive yarn sensor schematics, and picture b) conductive fibres substituted to normal threads in the braid and relative electric circuit

Similarly, also Felt et al., developed a reinforcing smart braid, Fig. 38, constituted by conductive insulated wires. [70] This braid needs to be mounted externally, and this might add some complexities to the fabrication process. The contraction is determined through the measure of the circuit inductance variation.

The last solution that will be presented in this work, is probably the less adequate one, but the most bioinspired. Shin et al., indeed, tried to mimic the nervous system, controlling the spinal reflexes, by coupling a tension sensor, acting as a Golgi tendon, and a length sensor, as muscle spindle. The sensor measures the contraction by relating it to the inclination angles between the central axis and the tangent to the inflated chamber. [71] This is made possible just by the use of a magnet and an IC magnetic field sensor,

measuring the variation of magnetic field flux density. Fig. 39 shows the operating principle and the overall system.

While it reportedly has a good accuracy, and takes inspiration from the nature, the applicability to our system, remains unlikely.
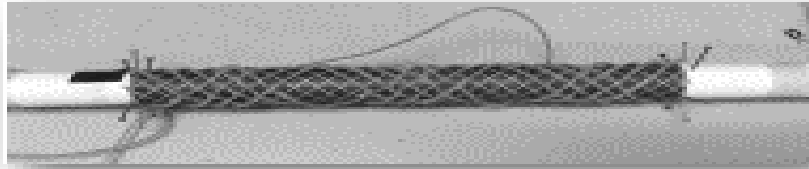

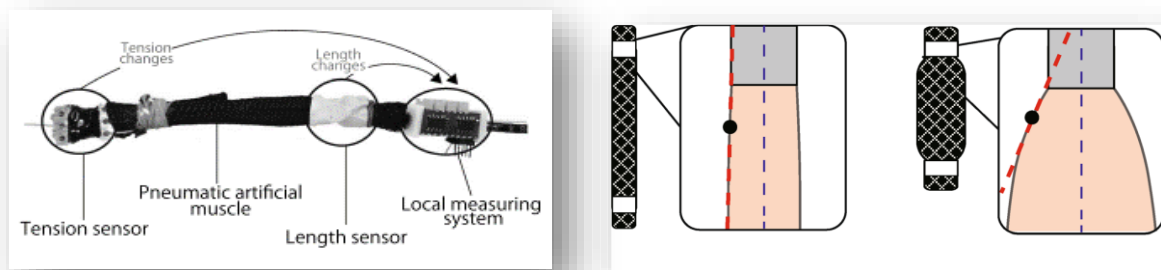*Fig. 38 The smart reinforcing braid.*

Fig. 39 Bioinspired sensing based on magnetic field changes.

To summarize the exposed technologies and underline their working principles Tab. 8 was produced. It can be noticed that most of the sensors are piezo-resistive. Although none of them has been tested yet, the solutions that are merging the actuation and sensing principles, besides presenting better performances, will probably be the preferred one in future, since they do not overcomplicate the system, by introducing different parameters, apart from the already known ones, thanks to the available McKibben geometrical models.

In Fig. 40, a tentative scheme of the foreseen control strategy is shown. Two are the main control loops that should be taken into consideration: the first one, aimed to the control of the overall system stroke volume, while a second one, aims to provide information about the contractile functionality of the actuators. The scheme gives an idea about both high and low-level control systems. Assuming that one could understand the level of activity of a person, a control on the final ejected volume can be hypothesized. Then, if the series of actuators is able to perform part of the control scheme computations,

thanks to its specific design and arrangement, the lower level control strategy can coincide with the basic contracting unit one, exactly as it happens in nature. In the heart indeed, the level of activity of a person influences directly the shortening frequency of the single myocyte, resulting in an overall system pulsing frequency increase, and thus a higher average stroke volume value. [72]

Tab. 9 Soft sensing technologies for McKibben Pneumatic Muscles

| SENSOR	TYPOLOGY
Soft strain sensor with chipless wireless readout	Piezo-Capacitive
Electrolycra	Piezo-Resistive
Dielectric elastomeric sensor	Piezo-Capacitive
Nylon carbon string with slider	Piezo-Resistive
Flexible ring	Piezo-Resistive
Electroconductive yarn and polyurethane core	Piezo-Resistive
Conductive braided fibres	Piezo-Resistive
Smart reinforcement braid	Inductive
Artificial proprioceptors	Magnetic
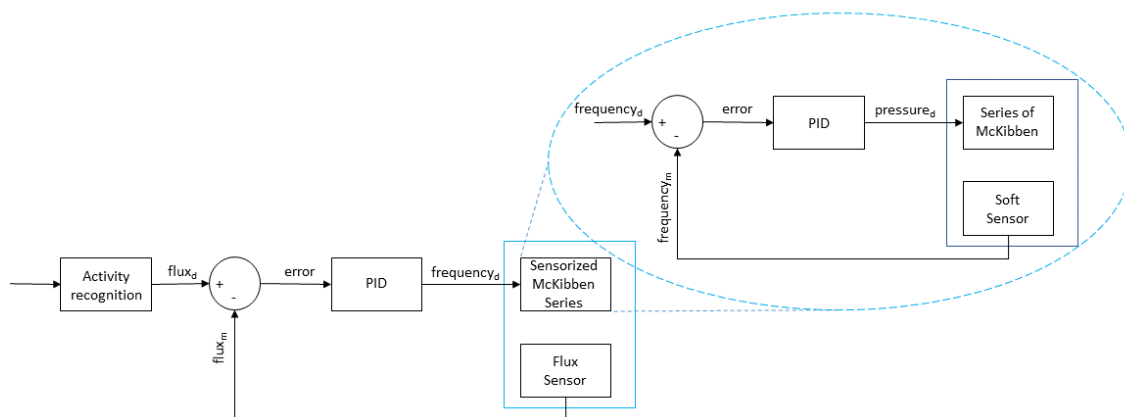
Fig. 40 Envisioned control scheme

7 Future works

Building a total artificial heart has been a big challenge, since centuries ago. For this reason, this work was aiming to give some guidelines for the development of a more bioinspired device. Indeed, most of the so far engineered devices are relying on working principles that are too far from the natural cardiac cycle, and thus have biocompatibility problems. Although not yet complete, the conducted study showed the immense artificially exploitable natural capabilities of smartly designed muscular band.

In order to validate its efficiency a geometrical model was built, although it was not possible to validate it yet, it gave important information about the right artificial muscle to be used. Moreover, it gave the possibility to foresee a simplification in the control strategy of the device: by merging an accurate model of a chamber and of the single actuator, the number of control parameters decreases significantly.

This particular characteristic could make it one of the most efficient devices, exactly as it is for our heart, being a self-regulating autonomous pump.

To get to this point, it would be important to keep in mind the overall device design and its fundamental requirements. The development of more functional ventricular chamber shape, through simulations, a detailed study on the pneumatic principles driving the series of actuators, but also the design of a functionalized disposition of the muscular band, are all envisioned future works. These studies could all lead to a more complex hardware structure, but an incredibly simplified control strategy, and, thus, provide this novel bioinspired actuation system with artificially-embodied intelligence.

8 Conclusion

Every year, heart failure affects more than 20 million people worldwide.

Every year, 45% of deaths are caused by ischemic heart related diseases.

Although simple in principle, the functionality of our hearts is still not permanently replaceable by an artificial device. Engineers, clinicians, biologists, and more in general, scientists made multiple efforts in this direction, presenting many different possible solutions: yet, none of them has been deemed sufficiently reliable. Urgent, strongly interdisciplinary, but most of all, challenging, the idea of a future fully biocompatible, soft robotic total artificial heart caught immediately my attention, both as an insatiably curious person and as a mechatronics engineer.

For this reason, the aim of this thesis project was to find the most promising design tools for the development of an innovative type of soft artificial heart.

To achieve such a goal, I decided to take inspiration from the most creative and effective designer: the nature. Shape, functional arrangement, and properties of natural structures are usually combined together to provide embodied intelligence: the morphological complexity translates into simpler control strategies.

In particular, by closely studying the orientation of cardiac fibres in mammals, I was able to observe the proofs of the theories of Francisco Torrent-Guasp, stating that the cardiac final pumping functionality is the result of a unique muscular band folded in a double helix, contracting in a timely and sequential manner.

To clarify the importance of these features, also from an engineering standpoint, I developed a simplified geometrical model of the ventricular chamber contraction.

Although it was not possible to completely validate it yet, it provided me with important information about the most suitable typology of actuators to be employed.

The importance of a high active/passive material ratio, stood out clearly: as it is in nature, both shortening, and thickening resulted to be fundamental to the goal. For this reason, McKibben, pneumatic artificial muscles were chosen as basic actuating element.

To get the best trade-off between ease in fabrication, durability, flexibility and shortening, I also conducted extensive studies on the most suitable materials to be used during the fabrication process.

Then, once the actuator unit was chosen, always keeping an eye on the natural myocardial tissue, I thought about the design of a smart, but passive, connective element. By connecting the actuators in series, I qualitatively observed that it can be possible to obtain a timely sequential activation, just by exploiting a reduction in diameter between connective element and actuators. This observation brought me to some overall mechatronics related considerations.

Indeed, if the connective elements are smartly engineered, the final control of the device could be partly embedded, as it is in nature, in the designed device itself. For the other part, instead, it could be possible to exploit some of the soft sensing techniques that were developed so far, and maybe optimize them towards the goal.

In conclusion, I would like to underline the innovation brought up by this work in the mechatronics field. Indeed, I am firmly convinced that bio-inspiration could take the engineering design of our artificial devices to a completely new level: providing them with additional intelligence, that so far was not taken into consideration.

Nature, even in all its imperfections, gives us every day some incredibly smart examples of design: now it is up to us, as engineers and skilled researchers, to understand them, and optimize them, to keep the innovation progressing continuously towards a better everyday life.

9 References

[1] Iaizzo, P. A. (Ed.). (2009). *Handbook of cardiac anatomy, physiology, and devices*. Springer Science & Business Media.

[2] Carroll, J. D. (2005). Assessment of normal and abnormal cardiac function. *Braunwald's Heart Disease.*, *1*, 491-507.

[3] Ambrosy, A. P., Fonarow, G. C., Butler, J., Chioncel, O., Greene, S. J., Vaduganathan, M., ... & Gheorghiade, M. (2014). The global health and economic burden of hospitalizations for heart failure: lessons learned from hospitalized heart failure registries. *Journal of the American College of Cardiology*, *63*(12), 1123-1133.

[4] Mozaffarian, D., Benjamin, E. J., Go, A. S., Arnett, D. K., Blaha, M. J., Cushman, M., ... & Howard, V. J. (2015). Heart disease and stroke statistics—2016 update: a report from the American Heart Association. *Circulation*, CIR-0000000000000350.

[5] Wilkins, E., Wilson, L., Wickramasinghe, K., Bhatnagar, P., Leal, J., Luengo-Fernandez, R., Townsend, N. (2017). European Cardiovascular Disease Statistics. European Heart Network, Brussels, 192.

[6] "Cardiovascular Diseases (CVDs)." World Health Organization, World Health Organization, 19 Apr. 2018, www.who.int/cardiovascular_diseases/en/.

[7] Roth, G. A., Forouzanfar, M. H., Moran, A. E., Barber, R., Nguyen, G., Feigin, V. L., ... & Murray, C. J. (2015). Demographic and epidemiologic drivers of global cardiovascular mortality. *New England Journal of Medicine*, *372*(14), 1333-1341.

[8] Everly, M. J. (2008). Cardiac transplantation in the United States: an analysis of the UNOS registry. *Clinical transplants*, 35-43.

[9] Wilhelm, M. J. (2015). Long-term outcome following heart transplantation: current perspective. *Journal of thoracic disease*, *7*(3), 549.

[10] Rosenberg, G., & Bronzino, J. (1995). Artificial heart and circulatory assist devices. *Biomedical Engineering Handbook*, 1839-1846, pp. 63(1-8).

[11] Rodriguez, L. E., Suarez, E. E., Loebe, M., & Bruckner, B. A. (2013). Ventricular assist devices (VAD) therapy: New technology, new hope?. *Methodist DeBakey cardiovascular journal*, *9*(1), 32.

[12] Gerosa, G., Gallo, M., Bottio, T., & Tarzia, V. (2016). Successful heart transplant after 1374 days living with a total artificial heart. *European Journal of Cardio-Thoracic Surgery*, *49*(4), e88-e89.

[13] John, R., Kamdar, F., Liao, K., Colvin-Adams, M., Boyle, A., & Joyce, L. (2008). Improved survival and decreasing incidence of adverse events with the HeartMate II left ventricular assist device as bridge-to-transplant therapy. *The Annals of thoracic surgery*, *86*(4), 1227-1235.

[14] Morshuis, M., Schoenbrodt, M., Nojiri, C., Roefe, D., Schulte-Eistrup, S., Boergermann, J., ... & Arusoglu, L. (2010). DuraHeart™ magnetically levitated centrifugal left ventricular assist system for advanced heart failure patients. *Expert review of medical devices*, *7*(2), 173-183.

[15] LaRose, J. A., Tamez, D., Ashenuga, M., & Reyes, C. (2010). Design concepts and principle of operation of the HeartWare ventricular assist system. *ASAIO Journal*, *56*(4), 285-289.

[16] Schmid, C., Tjan, T. D., Etz, C., Schmidt, C., Wenzelburger, F., Wilhelm, M., ... & Scheld, H. H. (2005). First clinical experience with the Incor left ventricular assist device. *The Journal of heart and lung transplantation*, *24*(9), 1188-1194.

[17] Khanwilkar, P., Bearnson, G., Miller, P., Lee, J., Geisler, J., Nelson, K., & Long, J. W. (2011). levacor Vad: System Development Leading to Initiation of Us Btt Clinical Trial: 50. *Artificial Organs*, *35*(8), A39.

[18] Schmitto, J. D., Hanke, J. S., Rojas, S. V., Avsar, M., & Haverich, A. (2015). First implantation in man of a new magnetically levitated left ventricular assist device (HeartMate III). *The Journal of Heart and Lung Transplantation*, *34*(6), 858-860.

[19] Khan, S., & Jehangir, W. (2014). Evolution of Artificial Hearts: An Overview and History. *Cardiology research*, *5*(5), 121.

[20] Cook, J. A., Shah, K. B., Quader, M. A., Cooke, R. H., Kasirajan, V., Rao, K. K., ... & Tang, D. G. (2015). The total artificial heart. *Journal of thoracic disease*, *7*(12), 2172.

[21] Carpentier, A., Latrémouille, C., Cholley, B., Smadja, D. M., Roussel, J. C., Boissier, E., ... & Méléard, D. (2015). First clinical use of a bioprosthetic total artificial heart: report of two cases. *The Lancet*, *386*(10003), 1556-1563.

[22] CARMAT SA, 2017, Annual Report [Online] Available: https://www.carmatsa.com/en/

[23] Dowling, R. D., Gray Jr, L. A., Etoch, S. W., Laks, H., Marelli, D., Samuels, L., ... & Frazier, O. H. (2004). Initial experience with the AbioCor implantable replacement heart system. *The Journal of thoracic and cardiovascular surgery*, *127*(1), 131-141.

[24] Cohn, W. E., Timms, D. L., & Frazier, O. H. (2015). Total artificial hearts: past, present, and future. *Nature Reviews Cardiology*, *12*(10), 609.

[25] Pelletier, B., Spiliopoulos, S., Finocchiaro, T., Graef, F., Kuipers, K., Laumen, M., ... & Tenderich, G. (2014). System overview of the fully implantable destination therapy—ReinHeart-total artificial heart. *European Journal of Cardio-Thoracic Surgery*, *47*(1), 80-86.

[26] Schumacher, C. M., Loepfe, M., Fuhrer, R., Grass, R. N., & Stark, W. J. (2014). 3D printed lost-wax casted soft silicone monoblocks enable heart-inspired pumping by internal combustion. *Rsc Advances*, *4*(31), 16039-16042.

[27] Roche, E. T., Wohlfarth, R., Overvelde, J. T., Vasilyev, N. V., Pigula, F. A., Mooney, D. J., ... & Walsh, C. J. (2014). A bioinspired soft actuated material. *Advanced Materials*, *26*(8), 1200-1206.

[28] Roche, E. T., Horvath, M. A., Wamala, I., Alazmani, A., Song, S. E., Whyte, W., ... & Kuebler, J. (2017). Soft robotic sleeve supports heart function. *Science Translational Medicine*, *9*(373), eaaf3925.

[29] Roche, E. T., Horvath, M. A., Alazmani, A., Galloway, K. C., Vasilyev, N. V., Mooney, D. J., ... & Walsh, C. J. (2015, August). Design and fabrication of a soft robotic direct cardiac compression device. In *ASME 2015 International Design Engineering Technical Conferences and Computers and Information in Engineering Conference* (pp. V05AT08A042-V05AT08A042). American Society of Mechanical Engineers.

[30] Mac Murray, B. C., An, X., Robinson, S. S., van Meerbeek, I. M., O'Brien, K. W., Zhao, H., & Shepherd, R. F. (2015). Poroelastic foams for simple fabrication of complex soft robots. *Advanced Materials*, *27*(41), 6334-6340.

[31] Loepfe, M., Schumacher, C. M., & Stark, W. J. (2014). Design, performance and reinforcement of bearing-free soft silicone combustion-driven pumps. *Industrial & Engineering Chemistry Research*, *53*(31), 12519-12526.

[32] Cohrs, N. H., Petrou, A., Loepfe, M., Yliruka, M., Schumacher, C. M., Kohll, A. X., ... & Stark, W. J. (2017). A soft total artificial heart—first concept evaluation on a hybrid mock circulation. *Artificial organs*, *41*(10), 948-958.

[33] Cianchetti, M., Licofonte, A., Follador, M., Rogai, F., & Laschi, C. (2014). Bioinspired Soft Actuation System Using Shape Memory Alloys. Actuators, 3(3), 226–244.

[34] Villanueva, A., Smith, C., & Priya, S. (2011). A biomimetic robotic jellyfish (Robojelly) actuated by shape memory alloy composite actuators. *Bioinspiration & biomimetics*, *6*(3), 036004.

[35] Coral, W., Rossi, C., Curet, O. M., & Castro, D. (2018). Design and assessment of a flexible fish robot actuated by shape memory alloys. *Bioinspiration & biomimetics*, *13*(5), 056009.

[36] Pelrine, R., & Kornbluh, R. (2008). Variable-Stiffness–Mode Dielectric Elastomer Devices. Advances in Science and Technology, 61, 192–201.

[37] De Greef, A., Lambert, P., & Delchambre, A. (2009). Towards flexible medical instruments: Review of flexible fluidic actuators. *Precision engineering*, *33*(4), 311-321.

[38] Rateni, G., Cianchetti, M., Ciuti, G., Menciassi, A., & Laschi, C. (2015). Design and development of a soft robotic gripper for manipulation in minimally invasive surgery: a proof of concept. *Meccanica*, *50*(11), 2855-2863.

[39] Majidi, C. (2014). Soft robotics: a perspective—current trends and prospects for the future. *Soft Robotics*, *1*(1), 5-11.

[40] Amend, J. R., Brown, E., Rodenberg, N., Jaeger, H. M., & Lipson, H. (2012). A positive pressure universal gripper based on the jamming of granular material. *IEEE Transactions on Robotics*, *28*(2), 341-350.

[41] Polygerinos, P., Correll, N., Morin, S. A., Mosadegh, B., Onal, C. D., Petersen, K., … Shepherd, R. F. (2017). Soft Robotics: Review of Fluid-Driven Intrinsically Soft Devices; Manufacturing, Sensing, Control, and Applications in Human-Robot Interaction. *Advanced Engineering Materials*, 19(12), 1–22.

[42] Torrent-Guasp, F., Ballester, M., Buckberg, G. D., Carreras, F., Flotats, A., Carrió, I., … Narula, J. (2001). Spatial orientation of the ventricular muscle band: Physiologic contribution and surgical implications. *Journal of Thoracic and Cardiovascular Surgery*, *122*(2), 389–392.

[43] Forterre, Y., & Dumais, J. (2011). Generating helices in nature. *Science*, *333*(6050), 1715–1716.

[44] Buckberg, G. D. (2002). Basic science review: The helix and the heart. *Journal of Thoracic and Cardiovascular Surgery*, *124*(5), 863–883.

[45] Marcé-Nogué, J., Fortuny, G., Ballester-Rodés, M., Carreras, F., & Roure, F. (2013). Computational modeling of electromechanical propagation in the helical ventricular anatomy of the heart. *Computers in Biology and Medicine*, *43*(11), 1698–1703.

[46] Grosberg, A., & Gharib, M. (2009). Computational models of heart pumping efficiencies based on contraction waves in spiral elastic bands. *Journal of Theoretical Biology*, *257*(3), 359–370.

[47] Grosberg, A., & Gharib, M. (2009). A dynamic double helical band as a model for cardiac pumping. *Bioinspiration & Biomimetics*, *4*(2), 26003.

[48] Enache, R., Popescu, B. A., Piazza, R., Muraru, D., Călin, A., Beladan, C. C., … Ginghină, C. (2015). Left ventricular shape and mass impact torsional dynamics in asymptomatic patients with chronic aortic regurgitation and normal left ventricular ejection fraction. *The International Journal of Cardiovascular Imaging*, *31*(7), 1315–1326.

[49] van Dalen, B. M., Kauer, F., Vletter, W. B., Soliman, O. I. I., van der Zwaan, H. B., ten Cate, F. J., & Geleijnse, M. L. (2010). Influence of cardiac shape on left ventricular twist. *Journal of Applied Physiology*, *108*(1), 146–151.

[50] Azhari, H., Beyar, R., & Sideman, S. (1999). On the human left ventricular shape. *Computers and Biomedical Research, an International Journal*, *32*(3), 264–282.

[51] Buckberg, G. D., Hoffman, J. I. E., Cecil Coghlan, H., & Nanda, N. C. (2015). Ventricular structure-function relations in health and disease: Part I. The normal heart. *European Journal of Cardio-Thoracic Surgery*, *47*(4), 587–601.

[52] Buckberg, G., Mahajan, A., Saleh, S., Hoffman, J. I. E., & Coghlan, C. (2008). Structure and function relationships of the helical ventricular myocardial band. *Journal of Thoracic and Cardiovascular Surgery*, *136*(3).

[53] Nakatani, S. (2011). Left Ventricular Rotation and Twist: Why Should We Learn? *Journal of Cardiovascular Ultrasound*, *19*(1), 1.

[54] Clark, R. B., & Cowey, J. B. (1958). Factors Controlling the Change of Shape of Certain Nemertean and Turbellarian Worms. *J Exp Biol*, *35*, 731–748. Retrieved from

[55] Brainerd, E. L. (2005). Muscle fiber angle, segment bulging and architectural gear ratio in segmented musculature. *Journal of Experimental Biology*, *208*(17), 3249–3261.

[56] Alexander, R. (1969). The orientation of muscle fibres in the myomers of fishes. *Journal of the Marine Biology Association of the United Kingdom*, *49*, 263–290.

[57] Azizi, E., Gillis, G. B., & Brainerd, E. L. (2002). Morphology and mechanics of myosepta in a swimming salamander (Siren lacertina). *Comparative Biochemistry and Physiology - A Molecular and Integrative Physiology*, *133*(4), 967–978.

[58] Coghlan, C., & Hoffman, J. (2006). Leonardo da Vinci's flights of the mind must continue: cardiac architecture and the fundamental relation of form and function revisited. *European Journal of Cardio-Thoracic Surgery*, *29*(SUPPL. 1), 4–17.

[59] Daerden, F., & Lefeber, D. (2002). Pneumatic artificial muscles: actuators for robotics and automation. *European journal of mechanical and environmental engineering*, *47*(1), 11-21.

[60] Chou, C.-P., & Hannaford, B. (1996). Measurement and modeling of McKibben pneumatic artificial muscles. *Robotics and Automation, IEEE Transactions On*, *12*(1), 90–

[61] Davis, S., & Caldwell, D. G. (2006). Braid effects on contractile range and friction modeling in pneumatic muscle actuators. *International Journal of Robotics Research*, *25*(4), 359–369.

[62] Pillsbury, T. E., Kothera, C. S., & Wereley, N. M. (2015). Effect of bladder wall thickness on miniature pneumatic artificial muscle performance. *Bioinspiration & Biomimetics*, *10*(5), 055006.

[63] Stauffer, F., Zhang, Q., Tybrandt, K., Llerena Zambrano, B., Hengsteler, J., Stoll, A., … Vörös, J. (2018). Soft Electronic Strain Sensor with Chipless Wireless Readout: Toward Real-Time Monitoring of Bladder Volume. *Advanced Materials Technologies*, *3*(6), 1–7.

[64] Cianchetti, M., Renda, F., Licofonte, A., & Laschi, C. (2012). Sensorization of continuum soft robots for reconstructing their spatial configuration. *Proceedings of the IEEE RAS and EMBS International Conference on Biomedical Robotics and Biomechatronics*, 634–639.

[65] Goulbourne, N. C., & Son, S. (2007, January). Numerical and experimental analysis of McKibben actuators and dielectric elastomer sensors. In *ASME 2007 International Mechanical Engineering Congress and Exposition* (pp. 175-185). American Society of Mechanical Engineers.

[66] Hamamoto, I., Akagi, T., Dohta, S., & Matsushita, H. (2006, October). Development of a Flexible Displacement Sensor Using Nylon String Coated with Carbon and Its Application for McKibben Actuator. In *SICE-ICASE, 2006. International Joint Conference* (pp. 1943-1946). IEEE.

[67] Kuriyama, S., Ding, M., Kurita, Y., Ogasawara, T., & Ueda, J. (2009, October). Flexible sensor for Mckibben pneumatic actuator. In *Sensors, 2009 IEEE* (pp. 520-525). IEEE.

[68] Hirai, S. (2015, August). Measuring McKibben actuator shrinkage using fiber sensor. In *Robot and Human Interactive Communication (RO-MAN), 2015 24th IEEE International Symposium on* (pp. 628-633). IEEE.

[69] Misumi, J., Wakimoto, S., & Suzumori, K. (2015, December). Experimental investigation of conductive fibers for a smart pneumatic artificial muscle. In *Robotics and Biomimetics (ROBIO), 2015 IEEE International Conference on* (pp. 2335-2340). IEEE.

[70] Felt, W., & Remy, C. D. (2014). Smart braid: Air muscles that measure force and displacement. *IEEE International Conference on Intelligent Robots and Systems*, (Iros), 2821–2826.

[71] Shin, H., Saitoh, H., Kawakami, T., Yamanishi, S., Ikemoto, S., & Hosoda, K. (2016). Development of an embedded sensor system for pneumatic artificial muscle proprioceptors. *Artificial Life and Robotics*, *21*(4), 486-492.

[72] Wu, Y., Rasmussen, T. P., Koval, O. M., Mei-ling, A. J., Hall, D. D., Chen, B., ... & Song, L. S. (2015). The mitochondrial uniporter controls fight or flight heart rate increases. *Nature communications*, *6*, 6081.

10 Acknowledgements

11 Supplementary material index

- Geometrical model testing: setup and experiments: VID1
- McKibben Actuator testing: VID2
- McKibben Actuators series- folded configuration: VID3
- McKibben Actuators series- linear configuration: VID4
- Helical band: VID5
- Unfolded swine heart:IMG1-IMG7
- Manometer data sheet
- Ecoflex™ Series data sheet